TÉCNICO LISBOA

Nonlinear Aeroelastic Scaling Studies of High Aspect-Ratio Wings

Mónica Lima Coelho

Thesis to obtain the Master of Science Degree in

Aerospace Engineering

Supervisors: Prof. Fernando José Parracho Lau
Dr. Frederico José Prata Rente Reis Afonso

Examination Committee

Chairperson: Prof. Filipe Szolnoky Ramos Pinto Cunha
Supervisor: Prof. Fernando José Parracho Lau
Member of the Committee: Prof. André Calado Marta

November 2016

Acknowledgments

First of all I would like to start by thanking my advisors. Professor Fernando Lau for its guidance, support and availability, and Professor Frederico Afonso for always being there and by his indispensable assistance throughout the whole process.

I would also like to acknowledge the IDMEC (Instituto de Engenharia Mecânica) for funding and providing the opportunity to participate on the EASN 2016 conference.

To all my friends I would like to thank for always being patient and available in times of need, and for helping make the university such a good experience.

My final words of gratitude are addressed to my parents, sisters and grandparents, who always supported me, giving me everything I needed throughout my whole life.

Resumo

Com o objectivo de melhorar a performance das aeronaves através da redução do consumo de combustível, aumentou-se o alongamento das asas. Em testes experimentais, é necessário garantir que o modelo utilizado irá reproduzir a resposta aeroelástica escalonada da asa real. Para tal, é necessário desenvolver metodologias de escalonamento aeroelástico. Os efeitos da escolha das quantidades físicas e da abordagem utilizada para garantir semelhança modal (comparação directa entre modos de vibração e critério de garantia modal ajustado) são analisados. Duas metodologias (distribuição de massa e rigidez igualadas simultaneamente e sequencialmente) são utilizadas e comparadas. A opção de utilizar um modelo feito de material compósito laminado é também analisada. Uma metodologia é aplicada a uma asa mais complexa baseada na asa referência do Projecto NOVEMOR. Conclui-se que nem todos os conjuntos de quantidades primárias são úteis. Para modelos simples a metodologia sequencial não forneceu bons resultados. Foi possível utilizar material compósito para o modelo reduzido. A diferença nas abordagens para igualar os modos de vibração não foram significativas. Para a asa complexa obtiveram-se bons resultados.

Palavras-chave: Correspondência de Modos de Vibração, Critério de Garantia Modal Ajustado, Materiais Compósitos, Quantidades Físicas.

Abstract

In order to improve aircraft range through the reduction of fuel consumptions, the wings aspect-ratio (AR) has been increased. For experimental tests, the scaled model must replicate the desired scaled aeroelastic response of the full-size wing and so, aeroelastic scaling methodologies must be developed. The effects of the chosen primary quantities and of the modal matching approach are analysed using two modal matching approaches (direct modal matching and the Coordinate Modal Assurance Criterion, COMAC) and two scaling methodologies (mass and stiffness distribution matched simultaneously and sequentially), and the option of using a laminated composite beam for the reduced model is analysed. A scaling procedure was applied to a more complex wing model based on the EU FP7 Project NOVEMOR reference wing. Not all sets of primary quantities are usefull. For simple models, sequential matching of stiffness and mass distributions did not provide good results. It was possible to properly scale a simple full-size wing model to a reduced model with laminated composite material. The difference in the approaches for matching the mode shapes is not significant. For a more complex wing, good results were obtained.

Keywords: Modes Matching, Coordinate Modal Assurance Criterion, Composite Materials, Primary Quantities.

Contents

List of Tables

List of Figures

Nomenclature

Greek symbols

α	Angle of attack.
δ	Source strength.
Γ	Dihedral angle.
γ	Ratio of specific heat.
ε	Strain components.
$\{\epsilon\}$	Strain field.
θ	Ply fiber orientation.
κ	Reduced frequencies.
λ	Eigenvalue.
Λ_{LE}	Sweep angle.
μ	Doublet strength.
ν	Kinematic viscosity.
Φ	Velocity potential.
ϕ	Amplitude of nodal displacement.
Φ_∞	Free-stream velocity potential.
φ	Mode shape.
ρ	Density.
ρ_{f_i}	Fiber density of ply i.
σ	Stress components.
$\{\sigma\}$	Stress field.
υ	Poissons's ratio.

ω Angular frequency.

Roman symbols

$[A_i]$ Aerodynamic terms in EOM.

A, Aeq Constraints matrices.

A_{ij} Extensional stiffnesses.

AR Aspect-Ratio.

$[B]$ Strain-displacement matrix.

$[B_{NL}]$ Nonlinear component of strain displacement matrix.

b Span.

b_1 First-half span.

b_2 Second-half span.

B_{ij} Bending-extensional coupling stiffnesses.

$[\bar{C}]$ Global material coefficients matrix.

$[C]$ Local material coefficients matrix.

c Height of the cross section of the model, Chord of the airfoil.

$c(x)$, $ceq(x)$ Constraints vectors.

C_D Coefficient of drag.

C_f Friction coefficient.

c_f Elastic foundation modulus.

C_L Coefficient of lift.

C_M Coefficient of moment.

C_p Corrected pressure coefficient.

c_θ Cosine of ply fibre orientation angle.

C_{D_0} Coefficient of profile drag.

C_{D_f} Drag coefficient correction.

C_{D_i} Coefficient of induced drag.

c_{fun} Constraints function of the scaling methodologies.

$C_{L_{trim}}$ Trim lift coefficient.

$C_{p,0}$ Incompressible pressure coefficient.

$[D]$ Elasticity matrix.

$\{d\}$ Nodal displacements vector.

D Drag.

D_{ij} Bending stiffnesses.

E Young's modulus.

e Span efficiency factor.

E_1 Longitudinal Young's modulus.

E_2 Transverse Young's modulus.

E_3 Perpendicular Young's modulus.

$\{F\}$ Load vector.

$\{F_g\}$ Vector of gravitational terms.

F Correction value.

f Frequencies.

$f(x)$ Objective function.

f_φ Modes objective function considering direct modal matching.

f_{COMAC} Modes objective function considering COMAC.

$fcount$ Number of calls of the FE analysis function.

FF Form factor.

Fr Froude number.

$fval$ Minimum value of objective function.

$\{g\}$ Gravity acceleration vector.

G Shear modulus.

g Gravity acceleration constant.

I Second moment of area.

$[K]$ Stiffness matrix in EOM.

k_F Force scaling factor.

k_f Frequency scaling factor.

k_I Inertia scaling factor.

k_l Length scaling factor.

k_M Mass scaling factor.

k_t Time scaling factor.

k_U Velocity scaling factor.

k_ρ Density scaling factor.

L Lift.

l Length.

lb Lower boundary.

$[M]$ Mass matrix in EOM.

M Mach number.

m Mass.

$M.A.C.$ Mean aerodynamic chord.

M_∞ Free-stream Mach number.

M_{xx}, M_{yy}, M_{xy} Moment resultants.

$[N]$ Shape function matrix.

N Modes number.

n Vector normal to the surface.

n_{ply} Number of plies in the laminate.

N_{xx}, N_{yy}, N_{xy} In-plane force resultants.

NN Nodes number.

O_{f_i} Orientation of fiber of ply i.

$ObjFun$ Complete objective function of the scaling methodologies.

p Pressure.

q Distributed transverse load.

Q_y, Q_z Transverse force resultants.

$\{R\}$ Restoring forces vector.

R Specific gas constant.

r Distance between point and the source/doublet location.

Re Reynolds number.

$[S]$ Inverse matrix of local material coefficients matrix.

S Wing area.

S_B Surface boundary.

s_θ Sine of ply fibre orientation angle.

S_{ref} Wing reference area.

S_{wet} Wing wetted area.

$[T]_\sigma$ Transformation matrix for stress components.

$[T]_\varepsilon$ Transformation matrix for strain components.

T Kinetic energy, Temperature.

t Time.

t_c Caps thicknesses of the cross section of the model.

t_i Thickness of ply i.

$\{u\}$ Displacement field.

U Potential energy.

u Displacement.

ub Upper boundary.

V Velocity, Volume fraction.

t_w Webs thicknesses of the cross section of the model.

w Transverse deflection, Width of the cross section of the model.

W_{engine} Engine weight.

W_{TO} Take-off weight.

$\{x\}$ Vector of elastic degrees of freedom in EOM.

x_0 Initial design variables.

z_k Distance of the ply in relation to the center of the laminate.

Subscripts

b Break.

f Composite fiber.

$f, crit$ Critical volume fraction of fiber value.

$f, max, prac$ Practical maximum fiber content.

i Computational index.

LE Leading edge.

m Scaled model, Matrix material

new New complex wing.

$root$ Root.

ref Reference NOVEMOR wing.

t Target value, Tip.

$trim$ Trim condition.

w Full-size wing.

Superscripts

T Transpose.

Glossary

AR	Aspect-Ratio.
COMAC	Coordinate Modal Assurance Criterion.
DOF	Degrees-Of-Freedom.
DV	Design Variable.
EASA	European Aviaton Safety Agency.
EOM	Equations Of Motion.
ESL	Equivalent Static Loads.
FAA	U.S. Federal Aviation Administration.
FAR	Federal Aviation Regulations.
FE	Finite Element.
GS	Global Search.
HALE	High Altitude Long Endurance.
ISQ	Instituto de Soldadura e Qualidade.
JAR-25	Joint Aviation Requirements for Large Aeroplanes.
LABET	Laboratório de Termodinâmica e Aeronáutica.
PDE	Partial Diefferential Equations.
PID	Proportional-Integral-Derivative.
RMS	Root Mean Square.
SQP	Sequential Quadratic Programming.

Chapter 1

Introduction

1.1 Motivation

High aspect-ratio wings have been studied with the objective of improving aircraft performance, with respect to range and fuel consumptions. The wingtip of these wings has less area, which causes less vortex induced downwash, leading to less induced drag. For low speed aircrafts, the total drag coefficient, C_D, can be defined as the sum of profile drag coefficient, C_{D_0}, and induced drag coefficient, C_{D_i} [1]:

$$C_D = C_{D_0} + C_{D_i} = C_{D_0} + \frac{{C_L}^2}{\pi e AR}, \tag{1.1}$$

where C_L is the lift coefficient, e is the span efficiency factor, and AR is the aspect-ratio.

These wings produce less drag, hence reducing fuel consumption, and providing a higher lift-to-drag ratio, thus resulting in increased endurance [2]. Combining high-aspect-ratio and low structural weight results in very flexible wings that can suffer large deformations, leading to geometrical nonlinear behaviour and aeroelastic problems [3]. Because of that, the necessity to study these aeroelastic problems in order to prevent catastrophic structural failure due to aeroelastic phenomena, such as divergence or flutter, increases. In the development of these type of wings, the engineers must guarantee that these phenomena will not occur for any condition within the vehicle's flight envelope. As in every engineering project, the development of high aspect-ratio wings starts by defining some conceptual designs, which are analysed, compared and improved using computational methods. In a final stage of the project, the model that presents the best performance must be built and tested experimentally to verify the results obtained by the computational methods [4], which can be costly and time consuming. To reduce the costs and time, aeroelastic scaling is used. Its objective is to design a smaller, simpler, thus cheaper and easier to manufacture, wing structure model that can replicate the scaled aeroelastic response of the more complex full wing structure. With this being said, the development of accurate aeroelastic scaling methodologies is very important.

1.2 Topic Overview and State of the Art

All scaling methodologies derive from the non-dimensionalization of the system's governing Equations Of Motion (EOM) according to Buckingham's Π-theorem, that states that if there is a physical situation that can be represented by means of an equation involving a certain number n of physical variables S, then the original equation can be rewritten in terms of a set of dimensionless parameters Π_1,Π_2, ..., Π_{n-m} that are the $n - m$ independent products of the arguments S_1, ..., S_n [5]. The advantage of using dimensionless variables is that the problem is expressed in terms of the minimum number of variables, and the dimensionless equation of motion is completely unaffected by scale effects, so the values of the dimensionless variables must be the same for both the full size and scaled models. Typical dimensionless arguments used for aeroelastic scaling are: the aspect-ratio; reduced frequencies; Mach number; and Reynolds number [6].

Aeroelastic scaling is a combination of geometric scaling, structural scaling and aerodynamic scaling [7]. The first similarity laws for aeroelastic scaling were defined by Bisplinghoff *et al.* [6], in the 60's. According to Bisplinghoff [6], the three fundamental airplane properties for designing aeroelastic models are the distribution of structural stiffness, external shape, and the distribution of mass. Since then some authors have been developing, analysing and improving different aeroelastic scaling methodologies.

French [8] developed an approach for the stiffness design of aeroelastically scaled wind tunnel models. Structural mass was used as the objective function for stiffness matching, leaving more mass available for tuning the frequencies and mode shapes of the structure. Only four columns of the flexibility matrix were used to specify constraints, which proved to be acceptable. His results indicated that using structural optimization can result in a procedure that matches desired stiffnesses well, and that defining both upper and lower bound displacements unnecessarily complicates the optimization problem.

Later, French and Eastep [9] presented a model that uses constrained numerical optimization methods to modify a finite element representation of the model structure so that some measure of the difference between the calculated and desired responses is minimized. First, only the structure stiffness is matched; then, the element sizes are fixed and concentrated masses are added to obtain the desired modal response. This method proved to be easy to implement and resulted in relatively simple structures that accurately meet the mass and stiffness requirements. An example problem showed that scaled flutter velocity and frequency requirements can be satisfied and that the predicted flutter mechanism is correct as well.

In [10], Friedmann and Presente presented a two-pronged approach suitable for the general aeroelastic and aeroservoelastic scaling. In this approach, basic scaling requirements are established using typical cross-sectional information and dimensional analysis, resembling the classical approach that does not take into consideration possible nonlinearities. In parallel, solutions based on computer simulations are obtained for each aeroelastic or aeroservoelastic problem. Combining the results from classical approach and computer simulations, a set of expanded or refined aeroelastic scaling requirements is obtained.

Blair *et al.* [7] described how the classical aeroelastic scaling laws are applied when developing scaled models and developed a conceptual design of an aeroelastically scaled flight test model of a joined-wing High Altitude Long Endurance (HALE) concept.

Pereira *et al.* [11] described an aeroelastic scaling method to develop a scaled wing-tunnel test model for a joined-wing full size aircraft. The model was scaled such that its characteristics under steady loads match those of the full-scale aircraft, and also match normalized natural frequencies. Two approaches for achieving reduced frequencies similitude were examined: 1) design the scaled model to match scaled natural frequencies and natural mode shapes, so that in light of incompressible aerodynamics the reduced frequencies should match; 2) match both the scaled natural frequencies and reduced flutter frequency in an optimization of the scaled model. However, the results presented were obtained by matching the scaled natural frequencies only. The methodology for scaling follows the steps: 1) calculate natural frequencies and modes of vibration, and static deformations of the baseline model; 2) make the aeroelastic analysis of the baseline model; 3) calculate the geometric and dynamic parameters of the wind-tunnel model; 4) design the wind tunnel model as well as make the static and dynamic analysis; 5) compare all results of the wind-tunnel model with the objective parameters obtained by scale factors and modal analysis of the baseline model; 6) run an optimization process to reduce the discrepancies between objective parameters and the results. Finally, a wind-tunnel model was built and ground vibration tests were performed. With this methodology, it was possible to reproduce the scaled natural frequencies and scaled flutter speed of the full scale vehicle, but not the reduced frequencies. The ground vibration tests exhibited excellent correlation between the baseline and scaled models.

Bond *et al.* [12], demonstrated an aeroelastic scaling procedure that accounts for geometric nonlinearity by scaling the eigenvalue associated with the buckling load. They concluded that aeroelastic scaling requires the proper match of natural mode shapes, in addition to natural frequencies. However, matching the vibration eigenvalues and eigenvectors proved to have satisfactory results in matching aeroelastic response throughout the velocity profile. The method for scaling the nonlinear static results augmented the linear aeroelastic scaling, *i.e.*, matching scaled natural frequencies and mode shapes, by matching the scaled critical buckling eigenvalue, as well. With this approach the scaled model matched the static nonlinear response of the target model reasonably well up to 60% of the buckling load. Also, they concluded that it may be necessary to match the entire geometric stiffness matrix, or perhaps simply more vibration or buckling modes, to better scale nonlinear response.

In [13], Ricciardi *et al.* developed a new scaling methodology that uses direct matching of the nonlinear static response to account for geometric nonlinearities. The optimization is facilitated by an Equivalent Static Loads (ESL) approach. Natural frequencies and mode shapes are matched by optimizing nonstructural mass. The design failed to converge, the optimizer entered a pattern between two linear sub-optimal and two nonlinear solutions. Nevertheless, the objective function was successfully reduced by an order of magnitude. The methodology was successfully used to design a joined wingbox model to match the response of a joined wing beam model. Both the aeroelastic frequency and damping, and the nonlinear static responses matched well.

Later, Ricciardi *et al.* [14] developed a methodology for designing the nonlinear aeroelastically scaled models that uses direct matching of linear and nonlinear static responses, while simultaneously satisfying modal-frequency constraints. This method is evaluated by comparing the nonlinear aeroelastic response of the scaled model to the response of the target model and a scaled model designed using traditional

scaled-model design methods. The traditional method proved to have room for improvement. It satisfied the frequency constraints but there is a clear reduction in modal-frequency agreement in the deformed state. As for the new method, the designed model retains linearised frequency agreement with the target model.

Wan and Cesnik [3] demonstrated a methodology for geometrically nonlinear aeroelastic scaling of very flexible aircraft. The known linear scaling factors and similarity rules are extended to address geometrically nonlinear aeroelastic scaling. Two models are compared, one that considers Froude number similarity and Reynolds number similarity, and one that only considers Reynolds similarity. They concluded that it is imperative that the Froude number similarity be met.

Spada [2] employed three scaling methodologies: two classical scaling methodologies and developed a partially new nonlinear aeroelastic methodology. The first classical method (Method 1) does a direct modal response matching, while the second classical method (Method 2) uncouples the mass and stiffness distribution to achieve the modal response. The new developed method (Method 3) uses two different optimization routines to match the nonlinear static response and the mode shapes of the full model. This is the first demonstration of an optimization that simultaneously combines ESL for matching the nonlinear full model response with structural dynamic for a high-aspect-ratio wing of a commercial jet. The classical approaches presented a very similar average error, but Method 2 requires less computational time. Method 3 presented a smaller average error than the other two methods, but it needs more computational time than either of the classical approaches. Therefore, this method is not recommended when the structure does not experience nonlinear effects.

Tang *et al.* [15] studied the scaling laws of gust alleviation control system and the influence of different scaling choices of Froude number. Through theoretical demonstration, the scaling criterion of a classical Proportional-Integral-Derivative (PID) control system has been developed and a scaling methodology is provided and verified. They concluded that Froude number similarity could be quite important if the gravity provides one of the significant loads. Gravity could be avoided by mounting the model on the floor but in many practical cases the gravity is actually an important factor in gust related tests, so it is often recommended to match the Froude number.

1.3 Composite Materials in Aeroelasticity

In order to improve the stiffness of wings while still keeping low structural weight, composite materials are a good option, and have been widely used in the aircraft industry for many years. The properties of laminated composite materials can have an effect on the aeroelastic behaviour of high-aspect-ratio wings, and are being used to tailor and optimize these wings.

Shyprykevich [16] studied the interaction that two different graphite/epoxy anisotropic laminates can induce between wing bending and twist. The two laminates were used as covers for two subscale box beams. The results have indicated that the in-plane stiffness properties of anisotropic laminates can be predicted if the layer properties of the composite materials are accurately known. However, it can only have satisfactory results provided the limits of the laminate linear behaviour are not significantly

exceeded; therefore, it would not be possible to apply this to high-aspect-ratio wings.

Cesnik *et al.* [17], discussed, among other things, the importance of using the right stiffness formulation in order to model material couplings, the variations of divergence and flutter speeds with the changes in the lamination angle of a box-beam model of a wing cross section, and some of the effects of a nonlinear structural model on the aeroelastic stability of a slender wing.

Wan *et al.* [18] performed the aeroelastic modeling and calculation for high-aspect-ratio composite wings with different forward-swept angles and skin ply-orientations, to analyse the effects of forward-swept angle and skin ply-orientation on the static and dynamic aeroelastic characteristics.

Kameyama and Fukunaga [19], investigated the effect of laminate configuration on the flutter and divergence characteristics for composite plate wings. To examine the effect of laminate configuration, the flutter and divergence characteristics were represented on the lamination parameter plane.

Stodieck *et al.* [20] investigated the use of tow-steered composites to tailor the aeroelastic behaviour of composite wings. These composites have variable angle tow plies, in which the fibres follow a predefined curvilinear path such that the fibre angle and ply stiffness vary continuously through the plane of each ply. The aeroelastic behaviour of a simple rectangular unswept composite wing was modelled and symmetric lay-ups have been considered where the outer fibres are allowed to vary in orientation along the wing span. The effects on free vibration, flexural axis, flutter and divergence speeds, and gust loads were examined. They found that it is possible to influence the aeroelastic behaviour in both a beneficial and detrimental manner using tow steering. By increasing the design space, tow-steered laminates allow improved designs compared to traditional unidirectional composite laminates.

With this in mind, composite materials can also be a good option for scaled models, simplifying the inner structure but still maintaining the same aeroelastic behaviour as the full-scale model.

1.4 Thesis Outline

Chapter 1 starts by providing a motivation for the pursuit of better aeroelastic scaling methodologies. It follows by presenting an introduction of the theme and a review of the state of the art. Also, the influence of composite materials in aeroelastic tailoring of high-aspect-ratio wings is presented. Finally, a brief paragraph explains what it is necessary to certify, for fatigue evaluation, new components of an aircraft.

Chapter 2 presents the theoretical background of aeroelasticity, aeroelastic scaling, and composite materials.

In Chapter 3, two different scaling methodologies are described, that will be used throughout the thesis in different analysis. Also, a resumed explanation of some of the computational tools used is provided.

Chapter 4 consists in the first analysis, in which different sets of primary quantities for aeroelastic scaling are chosen, and the correspondent scaling factors defined, in order to evaluate their influence in the results by performing the scaling methodology in a simple model. The results are presente which contain a comparison between all sets, and also between the two methodologies and the two approaches

for matching the mode shapes. The Reynolds number similarity of the resulting models for all sets is also analysed.

In Chapter 5 a second analysis is described along with the results. This analysis consists in using a reduced model made of hybrid laminate composite materials, so that the possibility of using these type of materials in aeroelastic scaling is evaluated.

In Chapter 6, the final analysis is described. A more complex full-size wing model is defined, based on the EU FP7 Project NOVEMOR reference wing, to be scaled recurring to the best overall solution found with previous analysis. The results obtained are presented.

Finally, in Chapter 7, the conclusions and future work are discussed.

Chapter 2

Theoretical Background

2.1 Aeroelasticity

Aeroelasticity consists in the study of the mutual interaction between aerodynamic forces and elastic forces, and the influence of this interaction on airplane design [6]. It consists on a combination of: aerodynamic theories, that provide a prediction of the forces acting on a structure of a given shape; elasticity, that provides a prediction of the response of an elastic structure under a given load; and dynamics, that introduces the effects of inertial forces [4].

To classify aeroelastic problems, Collar [21] defined a triangle of forces (illustrated in Figure 2.1) that included aerodynamic, elastic, and inertial forces. Static aeroelastic phenomena involves only aerodynamic and elastic forces, and dynamic aeroelastic phenomena involves all three types of forces.

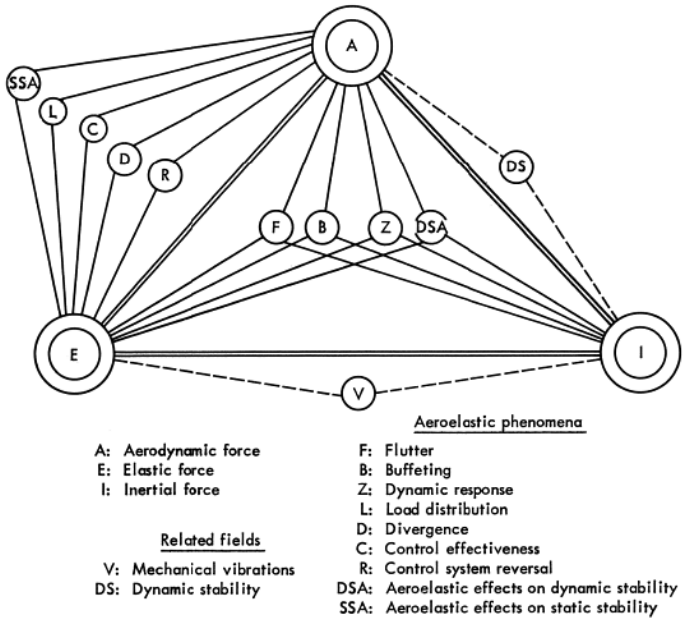

Figure 2.1: Collar triangle of forces [6].

These phenomena can diminish with time, converging to a condition of stable equilibrium, or may tend to diverge and destroy the structure. The most dangerous phenomena, depending on the design of

the wings, are divergence and flutter, because it can cause the structure destruction. Buffeting, control reversal, and limit cycle oscillation are other aeroelastic problems that can occur.

2.1.1 Divergence

Divergence is a static instability of a lifting surface of an aircraft in flight, at a speed called the divergence speed. When a wing reaches its torsional divergence speed, the increment in aerodynamic torsional moment due to an arbitrary increment in twist angle is exactly equal to the increment in elastic restoring torque. When the speed exceeds the torsional divergence speed, the increment in aerodynamic torsional moment exceeds the increment in elastic restoring torque, and the wing becomes statically unstable. This can be avoided with swept-back wings. By designing aircraft wings to be swept-back, the centre of twist moves forward and thus the offset between centre of twist and aerodynamic center is reduced, causing an increase in divergence speed. Therefore, divergence speeds of swept-back wings are not a matter of vital concern to the designer [6]. Despite that, if the aircraft presents a low sweep angle and high aspect-ratio wings this phenomenon should be analysed.

2.1.2 Flutter

Flutter is a dynamic instability occurring in an aircraft in flight caused by positive feedback between the body's deflection and the force exerted by the fluid flow, at a speed called the flutter speed, where the elasticity of the structure plays an essential part in the instability. At the flutter speed, the structure undergoes simple harmonic motion - zero net damping - and so any further decrease in net damping will result in a self-oscillation and eventual failure. It is most commonly encountered in bodies subjected to large lateral aerodynamic loads of the lift type. The classical type of flutter is associated with potential flow and usually, but not necessarily, involves coupling of two or more degrees of freedom, which causes the wing to cyclically increase in amplitude until it breaks which can occur in very few cycles. The non classical type of flutter, may involve separated flow, periodic breakaway and reattachment of the flow, stalling conditions, and various time-lag effects between the aerodynamic forces and the motion. Preventive measures usually involve either increased stiffness or decreased coupling by adjustments in mass distribution, or a combination of both. Wing planform and aspect-ratio also have significant effects on flutter characteristics. Decreases in wing aspect ratio and increases in sweep tend to raise flutter speeds, whereas increases in AR and decreases in sweep, including sweep forward, reduced flutter speeds [6], meaning that for high AR wings design, flutter is a matter of concern.

2.1.3 Buffeting

Buffeting consists in transient vibrations of aircraft structural components due to aerodynamic impulses produced by the wake behind wings, nacelles, fuselage pods, or other components of the airplane. A serious buffeting phenomenon confronting designers is encountered by fighter aircraft during pull-ups at high speed. This often results in rugged transient vibrations in the tail due to aerodynamic impulses from the wing wake [6].

2.1.4 Control Reversal

Control reversal is a condition occurring in flight, at a speed called the control reversal speed, at which the intended effects of displacing a given component of the control system are completely nullified by elastic deformations of the structure. Considering an aileron, for which the function is to alter the lift of the wings, with down aileron the lift on the wing is increased and with up aileron is decreased. Thus a rolling moment is produced. However, the aileron deflection will also produce a twisting moment for down aileron deflections, or torque for up aileron deflections. Wing twisting moments due to deflected ailerons increase as the square of the speed, whereas elastic restoring torques remain the same. Thus, as higher speeds are reached, the rolling moments become less, until a speed is reached where the aileron deflections will not produce a rolling moment. This speed is called the aileron reversal speed. Beyond this speed, the effect of ailerons is actually reversed [6].

2.1.5 Limit Cycle Oscillation

Limit cycle oscillation is a sustained periodic oscillation due to nonlinear aeroelastic interaction between the structure and the fluid, in which the wing behaves similarly to a flutter situation, but does not diverge. One or more nonlinearities, such as geometric, aerodynamic, stiffness, or structural damping, in the system act to limit the amplitude of the motion [22]. If the amplitude is large enough, the motion can damage the aircraft or stores attached to the wings [23].

2.2 Aeroelastic Scaling

2.2.1 Equations of Motion

For the EOM, a simplified physics model was chosen: the small disturbance, linear potential Partial Differential Equations (PDE) [24]:

$$[M]\{\ddot{x}\} + [k]\{x\} = [A_k]\{x\} + [A_c]\{\dot{x}\} + [A_m]\{\ddot{x}\} + [M]\{F_g\}, \tag{2.1}$$

where $\{x\}$ is the vector of elastic degrees of freedom; $[k]$ is the stiffness matrix; $[M]$ is the mass matrix; $[A_i]$ are the aerodynamic terms, being the subscripts k, c and m the terms referent to stiffness, damping and mass, respectively; and $\{F_g\}$ is the vector of gravitational terms for the corresponding degrees of freedom.

When the EOM describing this system are non-dimensionalized, they yield a set of parameters that are used for scaling the baseline aircraft [24].

2.2.2 Scaling Factors

The selection of scaling factors is critical in any aeroelastic scaling model design, and must be the first step [3]. These scaling factors are a set of parameters used to map the full-size test point (stiffness, mass and geometry) to the reduced scale test point, and derive from the non-dimensional parameters of the

EOM that represents the physical problem as mentioned before. The parameters to be matched are those that are free after constraints are applied to the model up to the number of primary dimensions involved in the governing equations. For aeroelastic models the primary dimensions are: length (l), time (t), and mass (M) [7]. Based on the primary dimensions, a set of primary quantities, that contain the primary dimensions, must be selected. These primary quantities will be freely chosen and will define the rest of the scaling factors.

The scaling factors needed for the analysis of an aeroelastic scaled model are: length (k_l), time (k_t), frequency (k_f), mass (k_M), air density (k_ρ), velocity (k_V), force (k_F), and inertia (k_I). These consist in the ratio between the scaled model parameter value and the full-size wing parameter value.

2.2.3 Parameters to Match

To properly aeroelastically scale a full-size wing, four similarity criteria must be met, plus a fifth similarity for cases where the gravity plays an important role: geometrical similarity; dynamic similarity (mass and stiffness similarity); aerodynamic similarity; and Froude number similarity [3].

Geometrical similarity is obtained when the airfoil size ratios are the same as the length scaling factor, and the airfoil shape is the same. For the mass and stiffness similarity, mass and stiffness distributions of the scaled model should be proportional to those of the full-size wing according to the mass and stiffness scaling factor. Aerodynamic similarity is met when geometrical similarity is met, and Mach and Reynolds number between scaled and full-size models are consistent. Froude number determines the ratio of the deflection under steady gravitational load to deflection due to aerodynamic and inertial loads.

To accomplish the similarity of the previous criteria, the following parameters similarity should be achieved [13].

- Mach number M (aerodynamic similarity):

$$M = \frac{V}{\sqrt{RT\gamma}}, \tag{2.2}$$

  where V is the velocity, R is the specific gas constant, T is the temperature, and γ is the ratio of specific heat.

- Reynolds number Re (aerodynamic similarity):

$$Re = \frac{Vx}{\nu}, \tag{2.3}$$

  where V is the velocity of the airflow, x is the distance (chord length) and ν is the kinematic viscosity.

- Froude number Fr:

$$Fr = \frac{V}{\sqrt{bg}}, \tag{2.4}$$

  where V is the speed of the aircraft, b is the span of the wing and g is the gravity acceleration constant.

- External geometry (geometrical similarity)
- Frequencies f and mode shapes φ (dynamic similarity)
- Reduced frequencies κ(dynamic similarity):

$$\kappa = f\frac{b}{V}, \tag{2.5}$$

where f is the natural frequency, b is the span, and V is the velocity.

Mach and Reynolds number similarity can be optional [3]. Mach number can be difficult and dispendious to match in wind-tunnel testing and it is usually ignored. For low-speed flying wings that are very flexible, the flow is incompressible, so there should be an attempt of matching the Reynolds number (or at least get it close to match) [25]. All other parameters are required to match. Froude number is very important for highly flexible structures, where the inertial forces (gravity loads) have a considerable contribution. In high-aspect-ratio wings, it is imperative that the Froude number similarity be met according to Wan and Cesnik [3]. To accomplish that, the relation between the velocity and length scaling factors should be

$$Fr_m = Fr_w \Leftrightarrow \left(\frac{V}{\sqrt{bg}}\right)_m = \left(\frac{V}{\sqrt{bg}}\right)_w \Leftrightarrow \frac{V_m}{V_w} = \sqrt{\frac{b_m}{b_w}} \Leftrightarrow k_V = \sqrt{k_l}, \tag{2.6}$$

where the subscripts m and w corresponds to the scaled model and to the full-size wing, respectively.

The external geometry must be the same as the full-size model to guarantee the same aerodynamic response. Frequencies and mode shapes are mandatory, since it is required to attain the same dynamic response. Reduced frequencies similarity is also required in order to match the linear aeroelastic and flight dynamic response according to Ricciardi *et al.* [13].

2.3 Composite Materials

Composite materials are widely used in aerospace industries due to their enhanced resistance and lighter weight [26].

These materials consist of two or more materials which together produce desirable properties that cannot be achieved with any of the constituents alone. Most man-made composite materials are made from two materials: a reinforcement material called fibre and a base material, called matrix material. In these composites, fibres are the principal load-carrying members, and the matrix material keeps the fibres together, acts as a load-transfer medium between fibres, and protects fibres from being exposed to the environment. They are often made in the form of a thin layer called lamina or ply. Plies can be stacked in order to form structural elements such as bars, beams or plates. In order to achieve a desired strength and stiffness for a specific application, the fibre orientation in each lamina and the sequence of layers can be chosen [26].

Two assumptions are made when formulating the constitutive equations of a lamina: 1) a lamina is a continuum; *i.e.*, no gaps or empty spaces exist; 2) a lamina behaves as a linear elastic material.

The generalized Hooke's law for an anisotropic material under isothermal conditions is given as [26]:

$$\sigma_{ij} = [C]\varepsilon_{ij}, \Leftrightarrow \varepsilon_{ij} = [S]\sigma_{ij} \tag{2.7}$$

where σ_{ij} are the stress components, ε_{ij} are the strain components, $[C]$ is the stiffness matrix, and $[S] = [C]^{-1}$:

$$[S] = \begin{bmatrix} \frac{1}{E_1} & -\frac{v_{21}}{E_2} & -\frac{v_{31}}{E_3} & 0 & 0 & 0 \\ -\frac{v_{12}}{E_1} & \frac{1}{E_2} & -\frac{v_{31}}{E_3} & 0 & 0 & 0 \\ -\frac{v_{13}}{E_1} & -\frac{v_{23}}{E_2} & \frac{1}{E_3} & 0 & 0 & 0 \\ 0 & 0 & 0 & \frac{1}{G_{23}} & 0 & 0 \\ 0 & 0 & 0 & 0 & \frac{1}{G_{13}} & 0 \\ 0 & 0 & 0 & 0 & 0 & \frac{1}{G_{12}} \end{bmatrix} \tag{2.8}$$

Initially, $[C]$ matrix has 81 constants. However, there are 21 independent elastic constants for the most general hyperelastic material, due to stress and strain symmetries, and the material coefficients matrix symmetry itself. When materials possess one or more planes of material symmetry, the number of independent elastic coefficients can be reduced. Considering orthotropic materials, with three mutually orthogonal planes of symmetry, the number of constants is reduced to 9 in three-dimensional cases [26].

2.3.1 Local Referential

A unidirectional fiber-reinforced lamina is treated as an orthotropic material whose material symmetry planes are parallel and transverse to the fiber direction. Axis x_1 is parallel to the fibre, x_2 axis is transverse to the fibre direction in the plane of the lamina, and the x_3 axis is perpendicular to the plane of the lamina, as illustrated in Figure 2.2.

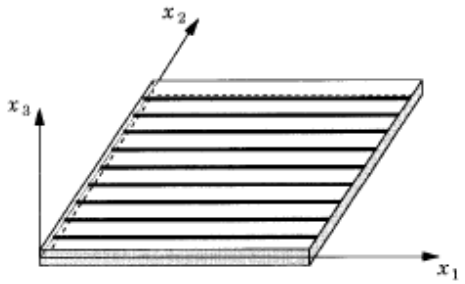

Figure 2.2: Local referential [26].

The theoretical approach used to obtain the orthotropic material properties of the lamina, called micromechanics, is based in the following assumptions [26]:

- Perfect bonding exists between fibres and matrix;
- Fibres are parallel, and uniformly distributed throughout;

- The matrix is free of voids or microcracks and initially in a stress-free state;
- Both fibres and matrix are isotropic and obey Hooke's law;
- The applied loads are either parallel or perpendicular to the fibre direction.

In order to determine the properties of each lamina, in the local referential, the rule of mixtures is used [26]. Subscripts f and m correspond to the fibre and matrix properties, respectively:

$$E_1 = E_m V_m + E_f V_f, \tag{2.9a}$$

$$\upsilon_{12} = \upsilon_f V f + \upsilon_m V_m, \tag{2.9b}$$

$$E_2 = \frac{E_f E_m}{E_f V_m + E_m V_f}, \tag{2.9c}$$

$$G_{12} = \frac{G_f G_m}{G_f V_m + G_m V_f}, \tag{2.9d}$$

where E_1 is the longitudinal modulus, E_2 is the transverse modulus, υ_{12} is the major Poisson's ratio, G_{12} is the shear modulus, V is the matrix and fibre volume fraction, and

$$G_{f,m} = \frac{E_{f,m}}{2(1 - \upsilon_{f,m})}. \tag{2.10}$$

Considering the material to be transversely isotropic the following relations can be applied:

$$E_3 = E_2, \tag{2.11a}$$

$$\upsilon_{13} = \upsilon_{12}, \tag{2.11b}$$

$$G_{12} = G_{13}. \tag{2.11c}$$

Additionally, any direction in plane 2-3 can be used as an axis, which means that the material can also be considered to be isotropic in plane 2-3:

$$\upsilon_{23} = \upsilon_{32} = \upsilon_m, \tag{2.12a}$$

$$G_{23} = \frac{E_2}{2(1 + \upsilon_{23})}. \tag{2.12b}$$

2.3.2 Global Referential

The global referential of the laminated composite is defined in Figure 2.3.

To formulate the problem of a laminated structure, the governing equations need to be written, with all their variables and coefficients, in the problem coordinates. It is necessary to obtain the transformation matrices so that it can be possible to calculate the global strain and stresses [26]:

$$\sigma_{local} = [T]_\sigma \sigma_{global}, \tag{2.13a}$$

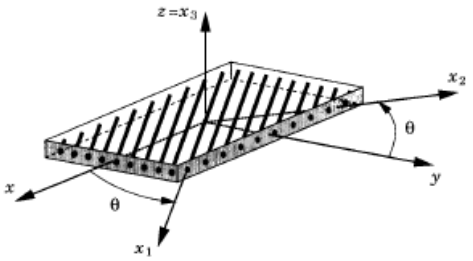

Figure 2.3: Global referential [26].

$$\varepsilon_{global} = [T]_{\varepsilon}\varepsilon_{local}, \tag{2.13b}$$

where:

$$[T]_{\sigma} = \begin{bmatrix} c_\theta^2 & s_\theta^2 & 0 & 0 & 0 & -2s_\theta \\ c_\theta^2 & s_\theta^2 & 0 & 0 & 0 & 2s_\theta \\ 0 & 0 & 1 & 0 & 0 & 0 \\ 0 & 0 & 0 & c_\theta & s_\theta & 0 \\ 0 & 0 & 0 & -s_\theta & c_\theta & 0 \\ s_\theta c_\theta & -s_\theta c_\theta & 0 & 0 & 0 & c_\theta^2 - s_\theta^2 \end{bmatrix}, \tag{2.14a}$$

$$[T]_{\varepsilon} = \begin{bmatrix} c_\theta^2 & s_\theta^2 & 0 & 0 & 0 & s_\theta c_\theta \\ c_\theta^2 & s_\theta^2 & 0 & 0 & 0 & -s_\theta c_\theta \\ 0 & 0 & 1 & 0 & 0 & 0 \\ 0 & 0 & 0 & c_\theta & -s_\theta & 0 \\ 0 & 0 & 0 & s_\theta & c_\theta & 0 \\ -2s_\theta & 2s_\theta & 0 & 0 & 0 & c_\theta^2 - s_\theta^2 \end{bmatrix}. \tag{2.14b}$$

In the previous equations $c_\theta = \cos\theta$, $s_\theta = \sin\theta$, and θ is the ply fibre orientation.

For the material stiffnesses C_{ij} the global matrix can be obtained with

$$[\bar{C}] = [T]_{\sigma}[C][T]_{\varepsilon}, \tag{2.15}$$

where $[\bar{C}]$ is the global material stiffness matrix and $[C]$ is the local material stiffness matrix.

In order to obtain the global elasticity properties, it is necessary to calculate the extensional stiffnesses A_{ij}, the bending stiffnesses D_{ij}, and the bending-extensional coupling stiffnesses B_{ij}. These are defined in terms of the lamina stiffnesses $\bar{C}_{ij}$ [26]:

$$A_{ij} = \sum_{k_1}^{n_{ply}} (\bar{C}_{ij})_k (z_k - z_{k-1}), \tag{2.16a}$$

$$B_{ij} = \sum_{k_1}^{n_{ply}} (\bar{C}_{ij})_k \frac{(z_k^2 - z_{k-1}^2)}{2}, \tag{2.16b}$$

$$D_{ij} = \sum_{k_1}^{n_{ply}} (\bar{C}_{ij})_k \frac{(z_k^3 - z_{k-1}^3)}{3}, \tag{2.16c}$$

where n_{ply} is the number of plies and z_k is the distance of the ply in relation to the centre of the laminate.

2.3.3 Symmetric Lay-up

Considering that the objective of using composite materials is to obtain a beam type scaled model that can replicate the same aeroelastic behaviour of a full-size wing, the lay-up of the laminate must be symmetric, which means that the material properties, locations, and lamination scheme are symmetric about the midplane, eliminating the coupling stiffnesses ($B_{ij} = 0$). By having isotropic layers, the relations between strains and resultants can be further simplified:

$$\begin{Bmatrix} N_{xx} \\ N_{yy} \\ N_{zz} \end{Bmatrix} = \begin{bmatrix} A_{11} & A_{12} & 0 \\ A_{12} & A_{11} & 0 \\ 0 & 0 & A_{66} \end{bmatrix} \begin{Bmatrix} \varepsilon_{xx}^{(0)} \\ \varepsilon_{yy}^{(0)} \\ \gamma_{xy}^{(0)} \end{Bmatrix}, \tag{2.17}$$

$$\begin{Bmatrix} M_{xx} \\ M_{yy} \\ M_{zz} \end{Bmatrix} = \begin{bmatrix} D_{11} & D_{12} & 0 \\ D_{12} & D_{11} & 0 \\ 0 & 0 & D_{66} \end{bmatrix} \begin{Bmatrix} \varepsilon_{xx}^{(0)} \\ \varepsilon_{yy}^{(0)} \\ \gamma_{xy}^{(0)} \end{Bmatrix}, \tag{2.18}$$

$$\begin{Bmatrix} Q_y \\ Q_z \end{Bmatrix} = \begin{bmatrix} A_{44} & 0 \\ 0 & A_{55} \end{bmatrix} \begin{Bmatrix} \gamma_{yz}^{(0)} \\ \gamma_{xz}^{(0)} \end{Bmatrix}, \tag{2.19}$$

where N_{xx}, N_{yy}, N_{xy} are the in-plane force resultants, M_{xx}, M_{yy}, M_{xy} are the moment resultants and Q_y, Q_z are the transverse forces resultant.

2.3.4 Hybrid Composites

Recently, the incorporation of several different types of fibres into a single matrix has led to the development of hybrid composites. These fibre-reinforced-plastic composites are used in thousands of structural applications such as aerospace, automotive parts, sports and recreation equipment, boats and office products, machinery *etc.* [27].

In automotive industry, the use of carbon fibres, which are much lighter, stronger and stiffer, remains low due to its high cost. So, to further reduce vehicle weight without excessive cost increase, one technique is to incorporate carbon fibre reinforcement into glass fibre composites [28].

Commercial aircraft applications are the most important uses of hybrid composites, since there is a need to lay greater stress on safety weight, and hybrid composites allow low structural weight combined with high stiffness at a lower price. Glass and carbon reinforced hybrid composites are the most desired materials [29].

Hybrid composites are materials made by combining two or more different types of fibres in a common matrix. They offer a range of properties that cannot be obtained with a single kind of reinforcement [27]. Their behaviour is a weighed sum of the individual components in which there is a more favourable

balance between the inherent advantages and disadvantages. Also, using a hybrid composite that contains two or more types of fibre, the advantages of one type of fibre could complement with what are lacking in the other [30]. As a consequence, a balance in cost and performance can be achieved through proper material design.

Chapter 3

Scaling Methodologies

In this work, two methodologies will be used: methodology 1 performs the matching of mass and stiffness distribution of the model and full-size wing simultaneously, while methodology 2 will first match the stiffness distribution and then the mass distribution. These methodologies are defined based on the parameters for which similarity must be met, which are listed in Section 2.2.3. Reynolds and Mach number similarity will only be evaluated after the scaling methodologies.

Before the optimization process, a Finite Element (FE) analysis must be performed to the full-size wing, to obtain the mode shapes, frequencies and displacements.

The optimization function used in both methodologies is *fmincon* from Matlab$^{\mathrm{R}}$; this function finds the minimum of a constrained nonlinear multi-variable function:

$$\min_{x} f(x) \text{ such that } \begin{cases} c(x) \leq 0 \\ ceq(x) = 0 \\ A \times x \leq 0 \\ Aeq \times x = 0 \\ lb \leq x \leq ub, \end{cases} \tag{3.1}$$

To define the *fmincon* function for this particular case, one needs to define: the objective function ($f(x)$), which is the function to be minimized; the initial value for the Design Variables (DV's) (x_0); the nonlinear constraints associated with the problem ($c(x)$); the upper and lower boundaries (ub and lb, respectively) that will restrict the design variables between two values; and the optimization options.

The algorithm chosen was the Sequential Quadratic Programming (SQP) which is a robust, efficient and reliable gradient-based optimization technique [31], where the function tolerance is defined as 1×10^{-8}.

3.1 Simultaneous Mass and Stiffness Distribution Matching

Optimization algorithm for the first methodology is represented in Figure 3.1. The input values include the initial design variables and the results obtained with the modal analysis of the full size wing model.

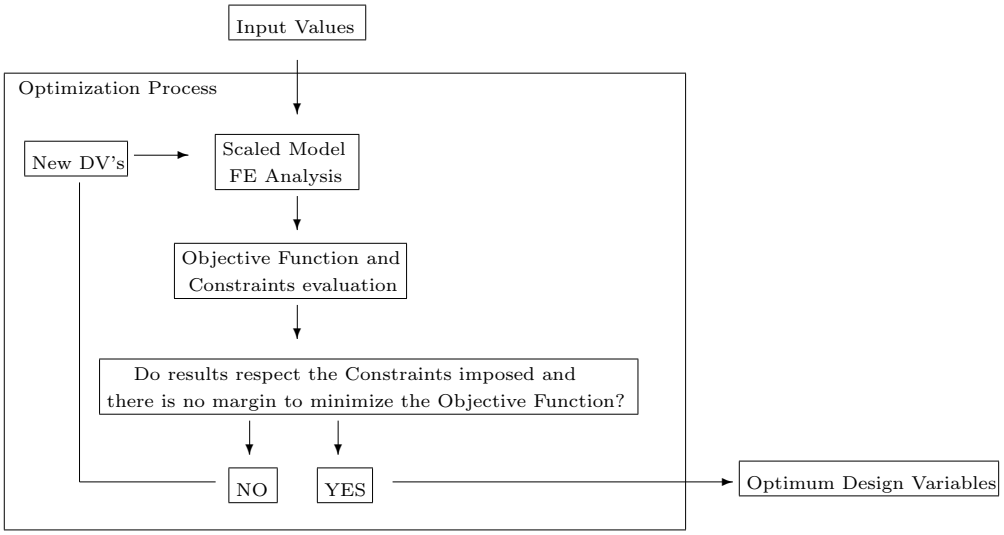

Figure 3.1: Scaling methodology algorithm 1.

With the initial design variables, the algorithm performs a FE analysis to obtain the mode shapes and frequencies of the scaled model, comparing the results with the target values (scaled values of the full-size wing FE analysis results). Then the design variables are iteratively updated using the optimization algorithm until the results match the objective values, minimizing the objective function and satisfying the constraints, resulting in the final optimum values for the design variables.

Objective Function

To match the stiffness and mass distribution, frequencies and mode shapes of the scaled model must match the ones of the full-size wing. The objective function is defined based on this requirement.

For the frequencies similarity, the absolute value of the difference between the target frequency and the model frequency is used:

$$f_{freq} = \sum_{i=1}^{N} |f_{i_m} - f_{i_t}|, \tag{3.2}$$

where N is the number of modes, f_{i_m} is the scaled model frequency of mode i and f_{i_t} is the target frequency of mode i.

For the mode shapes two methods are analysed: Coordinate Modal Assurance Criterion (COMAC), and direct modal matching. The COMAC attempts to identify which measurement degrees-of-freedom contribute negatively to a low value of Modal Assurance Criterion (MAC). The COMAC is calculated over a set of mode pairs: analytical versus analytical; experimental versus experimental; or experimental versus analytical. The two modal vectors in each mode pair represent the same modal vector, but the set of mode pairs represents all modes of interest in a given frequency range. For two sets of modes that are to be compared, there will be a value of COMAC computed for each (measurement) degree-of-freedom [32].

$$\text{COMAC} = \frac{|\ \varphi_m^T \times \varphi_t\ |^2}{(\varphi_m^T \times \varphi_m)(\varphi_t^T \times \varphi_t)}, \tag{3.3}$$

where φ_m corresponds to the mode shapes of the reduced scale model and φ_t to the target mode shapes,

which should be the same of the full-scale model.

To guarantee that the mode shapes match, COMAC has to result in an identity matrix $N \times N$, being N the number of modes. To accomplish that, the objective function is:

$$f_{\text{COMAC}} = |\sum_{i=1}^{N}(\text{COMAC}(i,i) - 1) + \sum_{i=1, i\neq j}^{N}\sum_{j=1, j\neq i}^{N}\text{COMAC}(i,j)| \tag{3.4}$$

For the direct mode matching the function is:

$$f_{\varphi} = |\varphi_m - \varphi_t| \tag{3.5}$$

The number of modes to match was defined as 5 for both the frequencies and mode shapes. By defining the number of modes as 5, the torsional stiffness was not properly matched. An attempt was made to include the first torsional mode, however the torsional stiffness is very difficult to achieve for simple models with a reduced number of design variables, thus the choice of only including the first 5 modes.

Finally, the objective function consists in the sum of the functions defined above:

$$ObjFun_1 = f_{freq} + f_{\text{COMAC}}, \tag{3.6}$$

or:

$$ObjFun_2 = f_{freq} + f_{\varphi} \tag{3.7}$$

Initial Design Variables

Optimization functions results are greatly influenced by the initial design variables, which means that it is very important to define them properly. Also, most optimization functions results consist in local minima and not global minima. Therefore different initial values are tested to try and obtain the global minima.

To further improve the optimization process, Global Search (GS) function of Matlab$^{\text{R}}$ is introduced. This function allows the *fmincon* function to be tested with different initial values, facilitating the search for the global minima, as the results obtained from all the different initial values are compared in order to determine the one which minimizes the objective function the most. GS uses a scatter-search mechanism for generating start points, analyses start points and rejects those points that are unlikely to improve the best local minimum found so far. For a description of the algorithm, see Ugray *et al.* [33].

Because of the fact that the Global Search algorithm does not use the same amount of initial points in every optimization process, it is possible to obtain the same minimum objective function value and DV's optimum solution, but with different computational time. To prevent this, the number of start points in Stage 1 (see Figure 3.2) was defined as 100 and the number of potential start points to examine in addition to x_0 was defined as 150, in order to force the number of initial start points of every scaling optimization to be the same, enabling a good analysis of the computational time. In the initial stage the default value was used for both parameters, in order to obtain the best initial point to use.

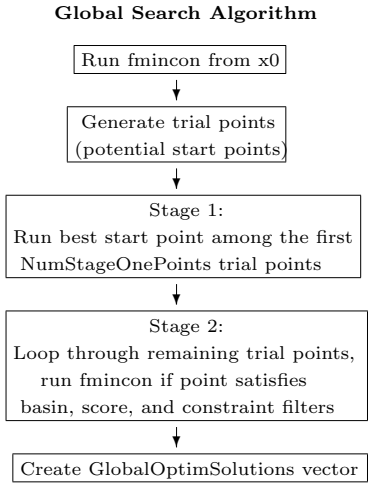

Figure 3.2: Global search algorithm [34].

Nonlinear Constraints

For the nonlinear constraints the difference between the dynamic frequencies is considered. The tolerance considered is of 5 %. The Root Mean Square (RMS) is used:

$$RMS_f = \sqrt{\frac{1}{N}\sum_{1}^{N}(f_{i_m} - f_{i_t})^2} \leq 5\% \tag{3.8}$$

And so the constraints are:

$$c_{fun} \leq \left(\sqrt{\frac{1}{N}\sum_{1}^{N}(f_{i_m} - f_{i_t})^2} - 0.05\right), \tag{3.9}$$

Boundaries

For the dimensions variables, the upper and lower boundaries will depend on the final results. Once we do not know the final dimensions *a priori* this feature is defined by trial and error. However, for some cases the design variables are constrained by other factors, such as the maximum percentage of fibres possible in a composite material, the limits of the orientation of the fibres in each ply ($-\pi/2$ and $\pi/2$), among others. When necessary, the boundaries are defined based on the constraints of each design variable.

3.2 Sequential Mass and Stiffness Distribution Matching

In methodology 2, the stiffness and mass distribution are matched sequentially. We start by matching the stiffness distribution. For this, we match the deformation of the reduced model with the scaled deformation of the full-size wing, by optimizing the dimensions of the section of the reduced model. Then, the mass distribution similarity is met by matching the scaled frequencies and modes. To do this,

5 mass points are added to the reduced model, in pre-determined locations along the beam model and equally spaced. The algorithm for this methodology is in Figure 3.3.

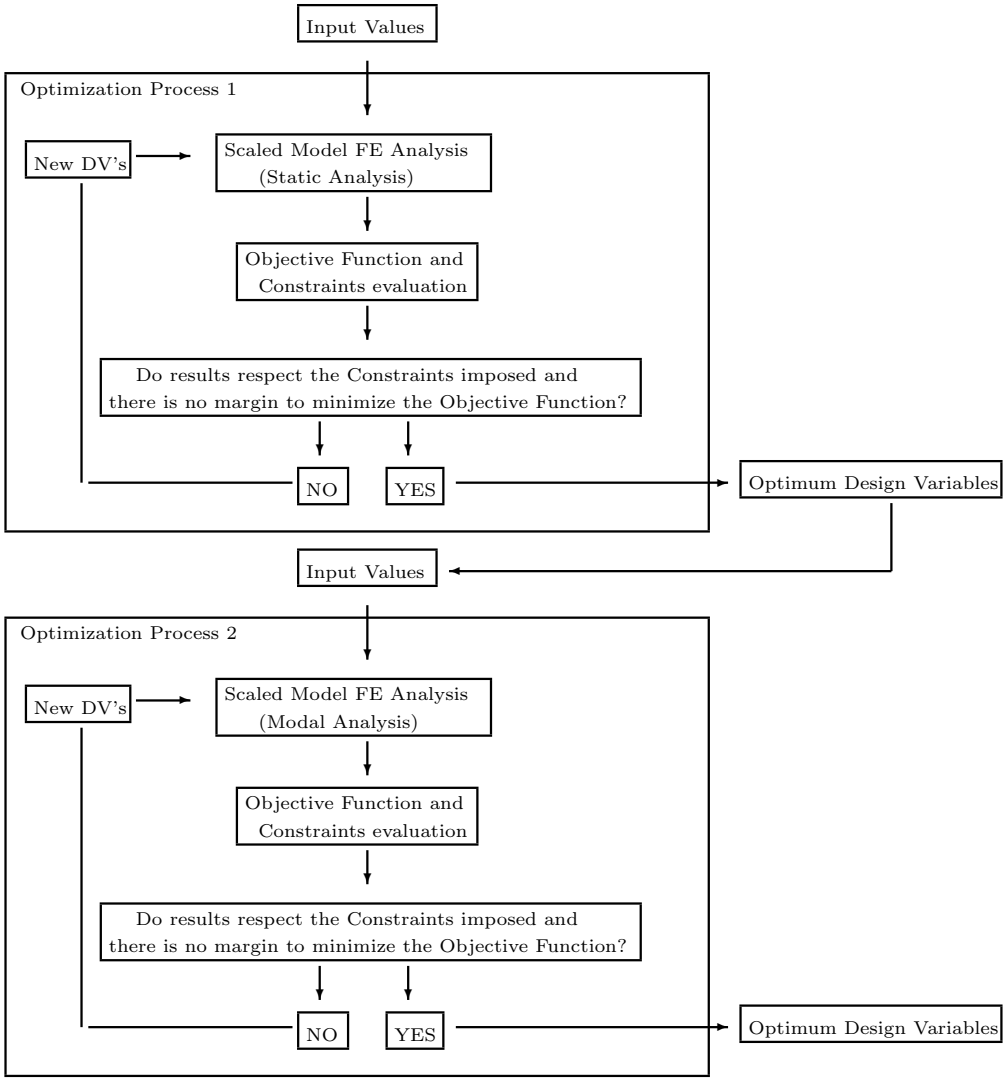

Figure 3.3: Scaling methodology algorithm 2.

Boundaries

The boundaries for both optimization processes of methodology 2 follow the same lines as the boundaries already described for methodology 1, meaning that when needed, the boundaries are applied. When there is no prior knowledge of the possible range of values of the design variables, the boundaries are defined by trial and error.

3.2.1 Optimization Process 1

In the first optimization process the stiffness distribution is matched, as mentioned before.

To do so, we first obtain the deformation of the full-size wing by imposing a pre-determined vertical force at the tip of the wing. The total deformation of each node consists in three translational components

and three rotational components. For the translational components, the length scaling factor is applied. Then, recurring to the initial design variables provided by the user, the same deformation analysis is performed to the scaled model, using a force that produces the desired deformation (a scaled value of the deformation used for the full-size wing). Both deformations are compared and the DV's values are iteratively optimized in order to reduce the objective function value, while respecting the constraints imposed.

Objective Function

The objective function is defined based on the difference of the reduced model deformation components, and the target values:

$$ObjFun = \sum_{i=1}^{NN} |(u_{i_m} - u_{i_t})|, \tag{3.10}$$

where NN is the number of nodes, u_{i_m} is the deformation of the reduced model for node i, and u_{i_t} is the target deformation for node i.

Initial Design Variables

The initial design variables for optimization process 1 are the section dimensions of the reduced model. Since these values are not known *a priori*, the initial point is defined by trial and error. As described in methodology 1, Global Search algorithm is used to accelerate the selection of the initial point.

Nonlinear Constraints

The constraint imposed to optimization process 1 is that the RMS of the deformation should be less than 5%:

$$RMS_f = \sqrt{\frac{1}{NN}\sum_{1}^{NN}(u_{i_m} - u_{i_t})^2} \leq 5\%. \tag{3.11}$$

So, the constraint function is:

$$c_{fun} \leq \left(\sqrt{\frac{1}{NN}\sum_{1}^{NN}(u_{i_m} - u_{i_t})^2} - 0.05 \right). \tag{3.12}$$

3.2.2 Optimization Process 2

Once the section dimensions are defined in the first optimization process, by matching the structural stiffness distribution, some masses will be added to the reduced model in order to match the mass distribution. To accomplish that, modal response of the scaled model must match the scaled modal response of the full-size wing. So, first the modal analysis is performed to the full-size wing. Then, the reduced model modal response (using the initial point provided) is calculated and compared to the scaled modal response of the full-size wing. This process continues until the design variables of the model result in the smallest possible objective function value and within the constraints imposed.

Objective Function

To guarantee that the mass distribution is properly scaled, frequencies and mode shapes of the reduced model must match the scaled frequencies and mode shapes of the full-size wing.

For the frequencies similarity, the absolute value of the difference between the target frequency and the model frequency is used. To match the mode shapes, we resort to the COMAC, since this method has proven to provide better results (see Section 4.5.1). So, the objective function is the one presented in Equation 3.6.

Initial Design Variables

The design variables for optimization process 2 are the radius and positions of the structural masses added to the reduced model.

Nonlinear Constraints

For the nonlinear constraints, the same option described in methodology 1 is considered, which corresponds to Equation 3.9.

3.3 Computational Tools

To perform the previously described methodologies and analyses some computational tools (which were already developed) were used, namely a structural and an aerodynamic model. In this section a brief explanation of these tools is provided.

3.3.1 Structural Model

To formulate the structural problem, Finite Element Method (FEM) is used. The structural model is a condensed 3D beam model, also known as "beam-like" model. Despite providing good structural responses results at low complexity and computational cost for aircraft design, it leads to some inaccuracies due to the direct application of beam elements to represent the wing. With this in mind, a more accurate model that accounts for structural stiffness and mass characteristics of "box-like" components (e.g. wingbox) was implemented and condensed in a "beam-like" model. Furthermore, for the study of high-aspect-ratio wings, the wing structure behaviour is similar to a "beam-like" structure. A wing-box is defined for each aerofoil section in terms of its chord-wise initial and final position, besides web and cap thicknesses. Using thin-wall theory and the parametrised wingbox data, the inertial properties (area and moments of inertia) and centroid are computed. The condensed beam model is then set to pass through the centroids of each aerofoil section. [35]

FEM is a numerical method in which a given domain is viewed as a collection of subdomains, and over each subdomain the governing equation is approximated by any of the traditional variational methods, making it easier to represent a complicated function as a collection of simple polynomials [36].

The finite element using in this work is a 3D thin/slender beam element based in Euler-Bernoulli beam theory and composed of two nodes with six degrees-of-freedom (DOFs) each [37].

After the problem is formulated, static and dynamic analysis can be done.

For static analysis, the system of equation takes the form:

$$[k]\{d\} = \{F\}, \tag{3.13}$$

yielding that the potential energy is stationary. By solving this equation we can obtain the displacements field.

For free vibration analysis, it is necessary to solve Equation (**??**) considering $F = 0$, meaning that the system is free of external forces:

$$[k]\{d\} + [M]\{\ddot{d}\} = 0 \tag{3.14}$$

The solution for the free vibration problem can be assumed as:

$$d = \phi \exp(i\omega t), \tag{3.15}$$

where ϕ is the amplitude of the nodal displacement, w is the (angular) frequency of the free vibration, and t is the time.

With the objective of enabling the model with the capability of incorporating geometric non-linearities, a few changes to both static and dynamic analyses need to be performed. To do so, the stiffness matrix becomes dependent of the deformed state, and an iterative method is required. The one implemented in the computational tool used is Newton-Raphson method [38], which aims at reaching the following equilibrium:

$${}^{t+\Delta t}\{F\} - {}^{t+\Delta t}\{R\}^i = \{0\}, \tag{3.16}$$

where the applied load, $\{F\}$, does not depend on the deformation, but the restoring force $\{R\}$ does, with i being the current iteration. The restoring forces are the internal structural nodal forces, which are computed from the previous iteration stiffness matrix as follows:

$${}^{t+\Delta t}\{R\}^i = {}^{t+\Delta t}\{K\}^{(i-1)}\{d\}^i \tag{3.17}$$

To treat large displacements and large rotations, NASTRAN$^{\text{TM}}$methodology [39] was followed, which consists in computing the net displacements and using the gimbal angle approach to treat, respectively, large displacements and large rotations.

Since gravity is important when studying high aspect-ratio wings due to the flexibility effects, the element weight is also considered in the model, and the gravity load, $\{F_g\}$ is computed by multiplying the mass matrix by the gravity acceleration vector, $\{g\}$ [35]:

$$\{F_g\} = [M]\{g\} \tag{3.18}$$

3.3.2 Aerodynamic Model

Panel methods are numerical schemes for solving the Prandtl-Glauert equation for linear, inviscid, irrotational, and incompressible flow about aircraft flying at subsonic or supersonic speeds [40]. The Prandtl-Glauert equation is the simplest form of the fluid-flow equations that contain compressibility effects, but neglecting all the viscous and heat transfer terms, assuming that the flow is irrotational, and discarding all nonlinear terms. Physically, these restrictions mean that important flow behaviour such as separation, skin-friction drag, and transonic shocks are not predicted with panel methods [40].

The formulation consists in the potential flow model implemented in the nonlinear aeroelastic framework [35] is based in the Katz and Plotkin formulation [41].

3.3.3 Aeroelastic Model

To properly couple the aerodynamic and structural solvers, in order to perform an aeroelastic analysis, the framework used to analyse the complex wing has a Fluid-Structure Interaction (FSI) algorithm capable of performing steady and unsteady calculations.

The FSI methodology can be classified as: (1) monolithic and (2) loosely coupled [42]. It is responsible for transferring the loads from the aerodynamic panels to the structure and transferring the structural displacements to the aerodynamic panels. Since the meshes are not coincidental (for fluid dynamics modelling a detailed mesh is required, as for structural dynamics modelling a relatively coarse mesh suffices [43]), a proper load and displacement transfer method is necessary.

The FSI is an iterative process which converges when equilibrium is reached, i.e. when both displacements and loads have converged. The convergence criteria is given by

$$\frac{1}{NN}\sum_{i=1}^{NN} \mid \frac{d_i^n - d_i^{n-1}}{d_i^n} \mid \leq 1 \times 10^{-7}, \tag{3.19}$$

where NN and d_i are, respectively, the number of structural nodes and nodal displacement (displacements and rotations) i, n is the current load step and $n-1$ the previous load step.

For the static aeroelastic calculations, a steady FSI algorithm is employed [35], which calculates the linear or non-linear static equilibrium position.

For the dynamic aeroelastic analyses, two methodologies were implemented [35]: (1) frequency domain, in which the flutter boundary is calculated at the linear or nonlinear equilibrium state (computed with the steady FSI algorithm) using the p-k method [44]; and (2) time domain, in which the unsteady FSI [35] is used to compute the nonlinear aeroelastic deformed state in time.

Chapter 4

Primary Quantities

The choice of the primary quantities can be influenced by different aspects. Depending on the type of experimental test that the model is intended for (wind-tunnel test or flight test), and on the test characteristics, some constraints will be added to the scaled model: span (due to the limited dimensions of the wind tunnel), wind speed, air density (it can be altered in wind-tunnel test but may prove expensive; for flight test the altitude can be defined based on this parameter but it can be challenging to achieve the exact value), thicknesses of the inner structure (structures that are too thin become more difficult to build and less resistant), among others.

With the objective of analysing the influence of the primary quantities choice in the scaling procedure, five different sets will be defined and applied to a simple model.

4.1 Full-Size Wing

The full-size wing to be scaled consists of a rectangular wing made of aluminium. In order to simplify the problem, the wingbox consists in a rectangular hollow beam, represented in Figure 4.1. The dimensions, material properties, and conditions of flight are presented in Table 4.1.

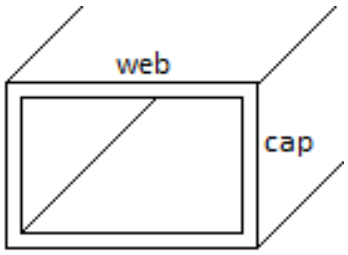

Figure 4.1: Full-size wing simplified wingbox.

4.2 Scaled Model

For the scaled model to have the same aerodynamic behaviour, it must have the same external shape as the full size wing. This feature can be accomplished by constructing an outer shell made of a lighter

Table 4.1: Full size wing dimensions, material properties, and flight condition.

Span (m)	20
Chord (m)	1
Web thickness (m)	0.01
Web length (m)	0.3
Cap thickness (m)	0.01
Cap length (m)	0.2
Material density (kg/m^3)	2700
Young's Modulus (GPa)	70
Shear Modulus (GPa)	26
Velocity (m/s)	40
Altitude (m)	0
Air density (kg/m^3)	1.225
Air kinematic viscosity (m^2/s)	1.46×10^{-5}

material, in order to maintain the desired mass distribution. The inner structure is the one that will provide, with a certain level of accuracy, the same aeroelastic behaviour of the full size wing.

Two different wingbox sections were tested for each set, in order to obtain the best result possible: the same hollow section as the full-size model (section 1), and a solid rectangular beam section (section 2).

The DV's vary for each wingbox section. For section 1 the DV's are the caps and webs thicknesses (t_c and t_w, respectively) and lengths (w and c, respectively), and for section 2, the DV's are the height and width (c and w respectively). The DV's are represented in Figure 4.2.

(a) Section 1 (hollow) DV's

(b) Section 2 (solid) DV's

Figure 4.2: Design variables for the two sections.

The material of the scaled model is also aluminium with the same properties as the full-size wing model, described in Table 4.1.

4.3 Scaling Factors

As mentioned before, the scaling factors will depend on the choice of the primary quantities. The sets that are going to be analysed are:

1. Density (ρ), Velocity (V), Span (b)

2. Kinematic Viscosity (ν), Span (b), Density (ρ)

3. Frequency (f), Mass (m), Span (b)

4. Kinematic Viscosity (ν), Density (ρ), Velocity (V)

5. Pressure (p), Span (b), Density (ρ)

Based on the SI units of each parameter, the scaling factors are defined combining the ratios of the primary quantities. Density has units of kg/m^3, velocity has units of m/s, span has units of m, kinematic viscosity has units of m^2/s, frequency has units of s^{-1}, mass has units of kg, and pressure has units of kg/ms^2. In the following section, the subscript m corresponds to the scaled model and the subscript w to the full-size wing.

For the velocity scaling factor, the priority is to match the trim condition of the full-size wing and, when the first option is not possible, the velocity scaling factor is defined based in the Froude similarity.

1. Density (ρ), Velocity (V), Span (b)

This set of primary quantities is the most widely used in aeroelastic scaling [3, 11] and can be used for wind-tunnel and flight test. With it, it is possible to select the desired span, velocity, and air density of the scaled model. These features are important in wind-tunnel testing because of the limited space, the added cost to changing air density, and the convenience provided by choosing the velocity of the test. This set is also important to flight tests because the density issue is even more difficult to tackle.

To begin, the length, time, frequency, mass and density scaling factors are defined:

$$k_l = \frac{b_m}{b_w}, \tag{4.1}$$

$$k_t = \frac{t_m}{t_w} = \frac{V_w}{V_m}\frac{b_m}{b_w} = \frac{1}{k_V}k_l, \tag{4.2}$$

$$k_f = \frac{f_m}{f_w} = \frac{T_w}{T_m} = \frac{1}{k_t} = k_V\frac{1}{k_l}, \tag{4.3}$$

$$k_m = \frac{m_m}{m_w} = \frac{\rho_m}{\rho_w}\left(\frac{b_m}{b_w}\right)^3 = k_\rho k_l^3, \tag{4.4}$$

$$k_\rho = \frac{\rho_m}{\rho_w}. \tag{4.5}$$

Velocity is one of the primary quantities, but in order for the scaled model to have the same trim condition as the full-size wing, the lift coefficient C_L must be the same.

Considering that the full-size wing and test model are in a steady flight condition, the lift L ratio is:

$$\frac{L_m}{L_w} = k_F, \tag{4.6}$$

$$k_F = \frac{\frac{\frac{1}{2}\rho_m V_m^2 S_m}{C_L}}{\frac{\frac{1}{2}\rho_w V_w^2 S_w}{C_L}} = k_\rho k_V^2 k_l^2, \tag{4.7}$$

$$k_V = \sqrt{\frac{k_F}{k_\rho k_l^2}}. \tag{4.8}$$

Since it is not possible to separate the velocity and force ratios, the force scaling factor is Equation 4.7, and the velocity scaling factor is calculated based on the Froude number similarity (see Equation 2.6):

$$k_V = \frac{V_m}{V_w} = \sqrt{k_l}. \tag{4.9}$$

Finally, the inertia scaling factor is defined:

$$k_I = \frac{\rho_m}{\rho_w}\left(\frac{b_m}{b_w}\right)^5 = k_\rho k_l^5. \tag{4.10}$$

2. Kinematic Viscosity (ν), Span (b), Density (ρ)

This set of primary quantities is suitable for wind-tunnel testing and flight tests. However one needs to verify the resulting air properties for the flight test. By defining the kinematic viscosity, it might be possible to match the Reynolds number, which can be important for small scaled models.

Although density and kinematic viscosity are both defined as primary quantities, only one can be truly defined, since they are related. Because of that, these features are defined prior to the Reynolds number matching.

$$k_\rho = \frac{\rho_m}{\rho_w}, \tag{4.11}$$

$$k_\nu = \frac{\nu_m}{\nu_w}. \tag{4.12}$$

To attempt matching the Reynolds number, the ratio between the length of the model and the wing is defined based on the definition of the Reynolds number (see Equation 2.3)

$$Re_m = Re_w \Leftrightarrow \left(\frac{Vx}{\nu}\right)_m = \left(\frac{Vx}{\nu}\right)_w, \tag{4.13}$$

$$k_l = \frac{l_m}{l_w} = \frac{k_\nu}{k_V}. \tag{4.14}$$

Analysing Equation (4.14), it is possible to see that to accomplish a scaled model span smaller than the full-size wing span, k_ν needs to be smaller than k_V.

Once again, the velocity must be constrained so that the model and the full-size wing has the same C_L. Starting with Equation (4.8), and replacing the force scaling factor from Equation (4.8), the velocity scaling factor is:

$$k_V = \frac{V_m}{V_w} = \frac{k_\nu}{k_l}. \tag{4.15}$$

Since the equation obtained for the velocity scaling factor is the same as for the length, the velocity scaling factor will be defined based on the Froude number similarity (see Equation (2.6)):

$$k_V = \frac{V_m}{V_w} = \sqrt{k_l}. \tag{4.16}$$

Replacing the velocity scaling factor from Equation (4.15) in the length scaling factor we obtain:

$$k_l = \frac{l_m}{l_w} = \sqrt[3]{k_\nu^2}. \tag{4.17}$$

Finally, the time, frequency, mass, force and inertia scaling factors are defined:

$$k_t = \frac{t_m}{t_w} = \frac{\nu_w}{\nu_m}\left(\frac{b_m}{b_w}\right)^2 = \frac{1}{k_\nu}k_l^2, \tag{4.18}$$

$$k_f = \frac{f_m}{f_w} = \frac{T_w}{T_m} = \frac{1}{k_t} = k_\nu\left(\frac{1}{k_l}\right)^2, \tag{4.19}$$

$$k_m = \frac{m_m}{m_w} = \frac{\rho_m}{\rho_w}\left(\frac{b_m}{b_w}\right)^3 = k_\rho k_l^3, \tag{4.20}$$

$$k_F = \frac{F_m}{F_w} = \frac{\rho_m}{\rho_w}\left(\frac{\nu_m}{\nu_w}\right)^2 = k_\rho k_\nu^2, \tag{4.21}$$

$$k_I = \frac{I_m}{I_w} = \frac{\rho_m}{\rho_w}\left(\frac{b_m}{b_w}\right)^5 = k_\rho k_l^5. \tag{4.22}$$

3. Frequency (f), Mass (m), Span (b)

This set can be applied to both wind-tunnel and flight test, although it requires to carefully analise which are the resulting speed V and density ρ. To start, the length, time, frequency, mass and density scaling factors are defined:

$$k_l = \frac{b_m}{b_w}, \tag{4.23}$$

$$k_t = \frac{t_m}{t_w} = \frac{f_w}{f_m} = \frac{1}{k_f}, \tag{4.24}$$

$$k_f = \frac{f_m}{f_w}, \tag{4.25}$$

$$k_m = \frac{m_m}{m_w}, \tag{4.26}$$

$$k_\rho = \frac{\rho_m}{\rho_w} = \frac{m_m}{m_w}\left(\frac{b_w}{b_m}\right)^3 = k_m\left(\frac{1}{k_l}\right)^3. \tag{4.27}$$

For the velocity we start with equation 4.8, and substitute the air density and force scaling factors to obtain:

$$k_V = \frac{V_m}{V_w} = k_f k_l. \tag{4.28}$$

In this case, the Froude number similarity is not considered.

Finally, the force and inertia scaling factors are defined:

$$k_F = \frac{F_m}{F_w} = \frac{m_m}{m_w}\frac{b_m}{b_w}\left(\frac{f_m}{f_w}\right)^2 = k_m k_l k_f^2, \tag{4.29}$$

$$k_I = \frac{I_m}{I_w} = \frac{m_m}{m_w}\left(\frac{b_m}{b_w}\right)^2 = k_m k_l^2. \tag{4.30}$$

4. Kinematic Viscosity (ν), Density (ρ), Velocity (V)

This set can be applied for both wind-tunnel and flight test. However one needs to evaluate the resulting span to verify if it is possible to perform the wind-tunnel test, and the resulting air properties for the flight test altitude.

Once again, kinematic viscosity and density depend on each other, and therefore only one is defined:

$$k_\nu = \frac{\nu_m}{\nu_w}, \tag{4.31}$$

$$k_\rho = \frac{\rho_m}{\rho_w}. \tag{4.32}$$

Reynolds number similarity attempt will be performed by defining the length scaling factor using Reynolds number definition. From Equation (4.13), results, once again:

$$k_l = \frac{b_m}{b_w} = \frac{k_\nu}{k_V}. \tag{4.33}$$

To obtain a span of the reduced model smaller than the span of the full-size wing, k_ν needs to be smaller than k_V.

Despite being one of the primary quantities, the velocity should, once again, be restrained to maintain the same trim condition, but it is not possible to apply this condition. Froude number similarity could be achieved, but a decision was made to define the scaled model velocity as a primary quantity, so that it is possible to reduce the length ratio through velocity. Therefore, the velocity scaling factor is:

$$k_V = \frac{V_m}{V_w}. \tag{4.34}$$

Finally, the time, frequency, mass, force and inertia scaling factors are:

$$k_t = \frac{t_m}{t_w} = \left(\frac{V_w}{V_m}\right)^2 \frac{\nu_m}{\nu_w} = \left(\frac{1}{k_V}\right)^2 k_\nu, \tag{4.35}$$

$$k_f = \frac{f_m}{f_w} = \frac{1}{k_t} = k_V^2 \frac{1}{k_\nu}, \tag{4.36}$$

$$k_m = \frac{m_m}{m_w} = \left(\frac{V_w}{V_m}\right)^3 \left(\frac{\nu_m}{\nu_w}\right)^3 \frac{\rho_m}{\rho_w} = \left(\frac{1}{k_V}\right)^3 k_\nu^3 k_\rho, \tag{4.37}$$

$$k_F = \frac{F_m}{F_w} = \frac{\rho_m}{\rho_w} \left(\frac{\nu_m}{\nu_w}\right)^2 = k_\rho k_\nu^2, \tag{4.38}$$

$$k_I = \frac{I_m}{I_w} = k_m k_l^2 = \left(\frac{1}{k_V}\right)^5 k_\nu^4 k_\rho. \tag{4.39}$$

5. Pressure (p), Span (b), Density (ρ)

This set of primary quantities can be applied to both wind-tunnel and flight test. Combining pressure and density, it is possible to select the material of the scaled model, one feature that normally is not properly scaled. First, the pressure, length, density, time, frequency and mass scaling factors are defined:

$$k_p = \frac{p_m}{p_w}, \tag{4.40}$$

$$k_l = \frac{b_m}{b_w}, \tag{4.41}$$

$$k_\rho = \frac{\rho_m}{\rho_w}, \tag{4.42}$$

$$k_t = \frac{t_m}{t_w} = \frac{p_w}{p_m} \frac{\rho_m}{\rho_w} \left(\frac{b_m}{b_w}\right)^2 = \frac{1}{k_p} k_\rho k_l^2, \tag{4.43}$$

$$k_f = \frac{f_m}{f_w} = \frac{1}{k_t} = k_p \frac{1}{k_\rho} \left(\frac{1}{k_l}\right)^2, \tag{4.44}$$

$$k_m = \frac{m_m}{m_w} = \frac{\rho_m}{\rho_w} \left(\frac{b_m}{b_w}\right)^3 = k_\rho k_l^3. \tag{4.45}$$

Once again, starting with Equation (4.8), and replacing the force scaling factor, yields:

$$k_V = \frac{V_m}{V_w} = \sqrt{\frac{k_p}{k_\rho}}. \tag{4.46}$$

in which the Froude number similarity is not considered.

Finally, the force and inertia scaling factors are defined:

$$k_F = \frac{F_m}{F_w} = \frac{p_m}{p_w}\left(\frac{b_m}{b_w}\right)^2 = k_p k_l^2, \tag{4.47}$$

$$k_I = \frac{I_m}{I_w} = \frac{\rho_m}{\rho_w}\left(\frac{b_m}{b_w}\right)^5 = k_\rho k_l^5. \tag{4.48}$$

The scaling factors of all the different sets of primary quantities are summarized in Table 4.2.

Table 4.2: Scaling factors for the five different sets of primary quantities.

Scaling Factors					
	Set 1	**Set 2**	**Set 3**	**Set 4**	**Set 5**
Parameters	ρ, V, b	ν, b, ρ	f, m, b	ν, ρ, V	p, b, ρ
Length k_l	$\frac{b_m}{b_w}$	$\sqrt[3]{k_\nu^2}$	$\frac{b_m}{b_w}$	$\frac{k_\nu}{k_V}$	$\frac{b_m}{b_w}$
Time k_T	$\frac{k_l}{k_V}$	$\frac{k_l^2}{k_\nu}$	$\frac{1}{k_f}$	$\frac{k_\nu}{k_V^2}$	$\sqrt{\frac{k_\rho k_l^2}{k_p}}$
Frequency k_f	$\frac{k_V}{k_l}$	$\frac{k_\nu}{k_l^2}$	$\frac{f_m}{f_w}$	$\frac{k_V^2}{k_\nu}$	$\sqrt{\frac{k_p}{k_\rho k_l^2}}$
Mass k_m	$k_\rho k_l^3$	$k_\rho k_l^3$	$\frac{m_m}{m_w}$	$\frac{k_\nu^3 k_\rho}{k_V^3}$	$k_\rho k_l^3$
Density k_ρ	$\frac{\rho_m}{\rho_w}$	$\frac{\rho_m}{\rho_w}$	$\frac{k_m}{k_l^3}$	$\frac{\rho_m}{\rho_w}$	$\frac{\rho_m}{\rho_w}$
Velocity k_V	$\sqrt{k_l}$	$\sqrt{k_l}$	$k_f k_l$	$\frac{V_m}{V_w}$	$\sqrt{\frac{k_p}{k_\rho}}$
Force k_F	$k_\rho k_V^2 k_l^2$	$k_\rho k_\nu^2$	$k_m k_l k_f^2$	$k_\rho k_\nu^2$	$k_p k_l^2$
Inertia k_I	$k_\rho k_l^5$	$k_\rho k_l^5$	$k_m k_l^2$	$\frac{k_\nu^5 k_\rho}{k_V^4}$	$k_\rho k_l^5$

Froude number similarity is met for Sets 1 and 2, and C_L trim similarity is met for Sets 3 and 5. Set 4 velocity scaling factor does not respect either condition.

The analyses will be made only for wind-tunnel tests. The initial values chosen for the primary quantities of the scaled model for Sets 1, 3 and 5 are listed in Table 4.3.

Table 4.3: Primary quantities values.

	Wind-Tunnel Test	Sets where this variables are defined
ρ_m (kg/m^3)	1.225	1, 5
b_m (m)	2	1, 3, 5
f_m (Hz)	Full-size wing frequencies	3
m_m (kg)	1	3
p_m (GPa)	70	5

The density chosen for the scaled model is the value correspondent to the air density at sea level. For wind-tunnel testing, it may prove challenging to alter the air density, so considering that the wind-tunnel installation is approximately at sea level, is an obvious choice.

The scaled model span is 2 m, which corresponds to a good size for most wind-tunnel installations

with about 2.7 m, without altering the characteristics of the flow in the airfoil: low-speed models may have a span as large as 75% of the test section width of the wind-tunnel [3].

The frequency value is defined based on the ability of measuring the values during the test. Values smaller than 1 Hz may be difficult to measure, and values that are too high can be affected by other factors. Knowing that the full-size wing frequencies are in an acceptable range, the frequency ratio is defined to be 1, meaning that the frequency values of the scaled model are the same as the full-size wing.

The mass value was chosen based on the necessity of transporting the model.

The pressure value is based on the attempt of approximating the scaled model material characteristics with the desired ones. By applying a scaling methodology allowing the material properties to vary, the results obtained often do not match any existing material. Usually, the material chosen for the scaled model is the one that resembles the most the desired characteristics. In this particular case, the scaled model material was chosen regardless of the density and pressure scaling factors for all sets except 5. Considering the desired material is aluminium, the value chosen for pressure consists on the Young's Modulus of aluminium, which in this case is the same as the full-size wing. Set 5 also has density as one of the primary quantities. By defining the air density of the model equal to the air density of the full-size wing, we are also defining the material density of the scaled model equal to the full-size wing. With both Young's Modulus and material density defined, the material of the scaled model is completely defined as aluminium.

For Sets 2 and 4, the kinematic viscosity and density of the air are defined together and related to the height considered for the flight condition. Also, since the span of the reduced model must be smaller than the full-size wing due to limitations of space in the tunnel, the kinematic viscosity ratio should be smaller than the velocity ratio. Considering an altitude of 0 m for both the reduced and the full-size wing, the kinematic viscosity ratio will be 1. For Set 2, since the velocity is limited by the similarity of the trim condition, the length scaling factor can only be altered by changing the kinematic viscosity scaling factor. For the flight condition defined for the full-size wing, there is no viable solution, and this set cannot be used. Since the intended objective of this analysis is to see whether or not this set can be effective in achieving Reynolds number similarity, we will assume, for Set 2 only, a different flight condition for the full-size wing, which is presented in Table 4.4, in order to guarantee a smaller span for the reduced model. For the primary quantities of Set 2, only the kinematic viscosity and density are defined. For Set 4 it is possible to select the reduced model velocity, and therefore to obtain a velocity scaling factor higher than 1 in order to have a reduced length scaling factor. Therefore for Set 4 the flight condition of the full-size wing does not need to be changed, and the velocity value is defined in addition to the air properties for the reduced model.

Table 4.4: Flight condition of the full-size wing for Set 2.

Velocity (m/s)	40
Altitude (m)	15000
Air density (kg/m^3)	0.1948
Air kinematic viscosity (m^2/s)	7.30×10^{-5}

The altitude chosen for the scaled model of Sets 2 and 4 is 0 m and the primary quantities values for

this altitude are listed in Table 4.5 along with the velocity value for the reduced model of Set 4.

Table 4.5: Primary quantities values for Sets 2 and 4.

Air density (kg/m^3)	1.225
Air kinematic viscosity (m^2/s)	1.46×10^{-5}
Velocity for set 4 (m/s)	100

Using the values chosen for the primary quantities the scaling factors can be obtained. They are listed in Table 4.6.

Table 4.6: Scaling factors for the five different sets of primary quantities.

Scaling Factors					
	Set 1	**Set 2**	**Set 3**	**Set 4**	**Set 5**
Parameters	ρ, V, b	ν, b, ρ	f, m, b	ν, ρ, V	p, b, ρ
Length k_l	0.1000	0.3420	0.1000	0.4000	0.1000
Time k_t	0.3162	0.5848	1	0.1600	0.1000
Frequency k_f	3.1623	1.7100	1	6.2500	10
Mass k_m	0.0010	0.2515	0.0039	0.0640	0.0010
Density k_ρ	1	6.2885	3.8580	1	1
Velocity k_V	0.3162	0.5848	0.1000	2.500	1
Force k_F	0.0010	0.2515	3.8580×10^{-4}	1	0.0100
Inertia k_I	1×10^{-5}	0.0294	3.8580×10^{-5}	0.0256	1×10^{-5}

4.4 Methodology

Since the objective of performing this scaling procedure is to analyse the influence of the primary quantities on the results, methodology 1 will be used for all sets.

For the constraints function the natural frequencies are used, as defined in Equation (3.9). For the modes matching, the two approaches will be used and compared using cross section 2 of the scaled model. Therefore, both objective functions defined in Equation (3.6) and Equation (3.7) will be evaluated for section 2. The upper and lower boundaries in this case are defined by trial and error.

In order to analyse the difference in the methodologies described, both methodologies will be applied to Set 1.

4.5 Results

The results obtained for all sets of primary quantities for section 1 and section 2, using COMAC, are presented in Tables 4.7 and 4.8, where *fval* corresponds to the minimum value of the objective function and *fcount* to the number of calls of the FE analysis function (which is called both in the objective

function and constraints function), and:

$$x_{section\,1} = x_{0_{section\,1}} = [w,\, c,\, t_w,\, t_c] \tag{4.49a}$$

$$x_{section\,2} = x_{0_{section\,2}} = [w,\, c] \tag{4.49b}$$

When considering Set 4 of primary quantities, the optimization process was unable to obtain a feasible solution that respected the constraints imposed using both sections, despite different values for the reduced model velocity were tested (always maintaining a velocity scaling factor higher than 1) and different optimization algorithms used (namely Genetic Algorithm). Therefore, only the results for the other sets are presented.

Table 4.7: Results for the five different Sets of primary quantities for section 1 using COMAC.

Section 1				
	x_0	x	*fval*	*fcount*
Set 1	[0.01000, 0.00650, 0.00064, 0.00055]	[0.00998, 0.00649, 0.00064, 0.00054]	0.02275	1505
Set 2	[0.05600, 0.04060, 0.00071, 0.00097]	[0.05573, 0.04082, 0.00071, 0.00100]	0.01804	1477
Set 3	[0.00344, 0.00230, 0.00053, 0.00037]	[0.00345, 0.00237, 0.00060, 0.00047]	0.02328	1477
Set 5	[0.03000, 0.02000, 0.00100, 0.00100]	[0.03000, 0.02000, 0.00100, 0.00100]	0.02149	781

Table 4.8: Results for the five different Sets of primary quantities for section 2 using COMAC.

Section 2				
	x_0	x	*fval*	*fcount*
Set 1	[0.01230, 0.00890]	[0.01228, 0.00894]	0.03831	985
Set 2	[0.07770, 0.05650]	[0.07769, 0.05653]	0.01809	1017
Set 3	[0.00388, 0.00283]	[0.00388, 0.00283]	0.02942	973
Set 5	[0.03890, 0.02830]	[0.03885, 0.02827]	0.02517	977

Section 1 results include thicknesses smaller than $1\,mm$, which can represent a problem with the manufacturing and the resistance of the model during the experimental test.

Comparing the results for sections 1 and 2, ignoring the manufacturability and resistance of the resulting model, considering that the priority is to have the smallest value possible for the objective function, but taking into account the number of function calls needed to obtain the results, some conclusions can be made.

For Set 1, despite the difference in function calls (34.55% more), the best overall result is obtained with section 1, due to the smaller objective function value (40.62% less), which compensates the increase in function calls. Set 2 has a smaller objective function value with section 1, but for less 31.14% function calls, the difference in the objective function value is not relevant (about 0.28%), and therefore the overall best result is obtained with section 2. For Set 3, section 1 provides the smaller objective function value (20.87% less than with section 2), which compensates the increase in the number of function calls (34.12% more), being this the best result. Finally for Set 5, section 1 provides a smaller objective function

combined with less function calls, being this the best result.

However, a smaller minimum value of the objective function does not necessarily means a better modal matching. This is due to the weight that each parameter to match has on the objective function: frequencies and COMAC. Achieving a minimum value for MAC does not necessarily means that the frequencies obtained for the reduced model are consistent with the target value. Because of that, a modal analysis is made to the reduced model recurring to the optimum DV's. This analysis is made for all sets and for both sections. The results are presented in Table 4.9.

Table 4.9: Frequencies comparison between the reduced frequencies of the scaled model and the target frequencies for each set and both sections considering COMAC.

			Natural Frequencies (Hz)				
			F1	F2	F3	F4	F5
Full-size wing			2.3044	3.1669	14.418	19.814	40.295
Mode shapes			1^{st} Flap	1^{st} Chord	2^{nd} Flap	2^{nd} Chord	3^{rd} Flap
Set 1	Section 1	Target	7.2873	10.015	45.594	62.658	127.42
		Scaled model	7.1207	10.414	44.552	65.156	124.511
		Difference (%)	2.2856	3.9863	2.2856	3.9863	2.2856
	Section 2	Scaled model	7.2883	10.011	45.600	62.637	127.42
		Difference (%)	0.0148	0.0337	0.0148	0.0337	0.0148
Set 2	Section 1	Target	3.9405	5.4153	24.654	33.882	68.903
		Scaled model	4.2296	4.9697	26.463	31.094	73.958
		Difference (%)	7.3365	8.2292	7.3365	8.2292	7.3365
	Section 2	Scaled model	3.9403	5.4152	24.653	33.881	68.899
		Difference (%)	0.0055	0.0021	0.0055	0.0021	0.0055
Set 3	Section 1	Target	2.3044	3.1669	14.418	19.814	40.295
		Scaled model	2.2964	3.2955	14.368	20.619	40.155
		Difference (%)	0.3480	4.0608	0.3480	4.0608	0.3480
	Section 2	Scaled model	2.3072	3.1632	14.435	19.791	40.342
		Difference (%)	0.1182	0.1180	0.1182	0.1180	0.1182
Set 5	Section 1	Target	23.044	31.669	144.18	198.14	402.95
		Scaled model	23.044	31.669	144.18	198.14	402.95
		Difference (%)	0.0000	0.0000	0.0000	0.0000	0.0000
	Section 2	Scaled model	23.047	31.673	144.20	198.16	403.00
		Difference (%)	0.0121	0.0107	0.0121	0.0107	0.0121

Analysing the results obtained for the modal analysis of each set and each section it is possible to conclude that section 2 provides a better result for all sets, except Set 5, which goes against the conclusions made based on the minimum objective function value for Sets 1 and 3.

Also, it is noteworthy to mention that, despite the difference in the frequencies being relatively small for all 5 mode shapes, since this 5 modes do not include the first torsion mode, the frequency of the first torsional mode of the reduced model does not match the frequency of the full-size wing for all sets except for Set 5 (for which the material is properly scaled). An attempt was made to include the first torsional mode, but with no good results.

Based on the modal analysis we concluded that the best result is obtained with section 2, except for Set 5. The final dimensions, material properties and condition of flight of the reduced model for each set of primary quantities are presented in Table 4.10. Also the best overall result of the objective function value and the number of function calls is listed.

Analysing the different primary quantity sets one can see that for this simple case, it is possible to

Table 4.10: Final dimensions and best overall result for each set using COMAC.

	Set 1	Set 2	Set 3	Set 5
w (m)	0.01228	0.07769	0.00388	0.03000
c (m)	0.00894	0.05653	0.00283	0.02000
t_w (m)	-	-	-	0.00100
t_c (m)	-	-	-	0.00100
b (m)	2	6.83990	2	2
ρ (kg/m^3)	2700	2700	2700	2700
E (GPa)	70	70	70	70
m (kg)	0.25920	0.25920	1	0.25920
ρ_{air} (kg/m^3)	1.22500	1.22500	4.72605	1.22500
ν_{air} (m^2/s)	1.46×10^{-5}	1.46×10^{-5}	4.6169×10^{-7}	1.46×10^{-5}
U (m/s)	12.64910	23.39200	4	40
fval	0.03831	0.01809	0.02942	0.02149
fcount	985	1017	973	781

obtain an approximately similar value for the objective function with all sets. Considering the parameter $fcount$, and comparing the best results for each set, there are no major differences. This means that all sets are plausible to be chosen, depending on the goal and type of experimental test.

However there are some constraints for Sets 2 and 3. Set 2 is restrained by the flight condition of the full-size wing for wind-tunnel tests, and by the dimensions of the tunnel, due to the necessity of accommodating the span of the scaled model in the installations. Set 3 resulted in air properties that do not correspond to any of the properties that are encountered in nature, at any height. Therefore, for this set to be used, it would be needed to alter the air properties inside the wind-tunnel, which can prove difficult to achieve.

4.5.1 Modal Matching Approach Analysis

In Table 4.11, the results obtained with direct modal matching for section 2 are presented.

Table 4.11: Results for the five different sets of primary quantities for section 2 using direct modal matching.

Section 2				
	x_0	x	*fval*	*fcount*
Set 1	[0.01230, 0.00890]	[0.01227, 0.00894]	0.12096	781
Set 2	[0.07770, 0.05650]	[0.07765, 0.05653]	0.03999	921
Set 3	[0.00390, 0.00280]	[0.00388, 0.00282]	0.10242	873
Set 5	[0.03890, 0.02830]	[0.03884, 0.02827]	0.03341	1045

It is possible to see that for all sets the results obtained for the objective function value are higher when using direct modal matching. However, it is not possible to directly compare these results due to the fact that, when directly comparing the modal vector, there are more points to be compared, which can lead to a higher objective function value. Analysing *fcount* it is possible to see that there are some differences in the number of function calls, being the function calls needed for direct modal matching inferior to the number of function calls needed for COMAC in most sets, except for Set 5, which needs

more function calls for direct modal matching (6.96%).

To evaluate which approach is better, we start by obtaining the optimum DV's with all decimal places for both approaches. Then, both optimum design variables (obtained with direct modal matching and COMAC) are used as the initial point for the COMAC modal matching approach, and the first objective function value registered. By comparing the first objective function value that each initial point provides, one can conclude which approach is better. The results are presented in Table 4.12.

Table 4.12: Comparison between the first objective function values obtained with the optimum design points for both approaches as initial points in the COMAC approach.

	First Objective Function Value		
	$x_0 = x_{COMAC\,modal\,matching}$	$x_0 = x_{direct\,modal\,matching}$	Best Approach
Set 1	0.0383	0.1328	COMAC
Set 2	0.0181	0.0493	COMAC
Set 3	0.0444	0.1160	COMAC
Set 5	0.0252	0.0462	COMAC

By analysing the results one can conclude that the COMAC modal matching approach is better for all sets.

Also the frequencies of the reduced model using both optimum DV's with all decimal places (obtained with COMAC and with direct modal matching) are compared to the target frequencies and the errors analysed in Table 4.13.

Table 4.13: Frequencies comparison for each set, using section 2 and considering COMAC and direct modal matching.

			Natural Frequencies (Hz)				
			F1	F2	F3	F4	F5
	Full-size wing		2.3044	3.1669	14.418	19.814	40.295
	Mode shapes		1^{st} Flap	1^{st} Chord	2^{nd} Flap	2^{nd} Chord	3^{rd} Flap
Set 1	COMAC	Target	7.2873	10.015	45.594	62.658	127.42
		Scaled model	7.2879	10.014	45.597	62.656	127.43
		Difference (%)	0.0081	0.0029	0.0081	0.0029	0.0084
	Direct	Scaled model	7.2894	10.007	45.607	62.608	127.46
		Difference (%)	0.0296	0.0798	0.0296	0.0798	0.0296
Set 2	COMAC	Target	3.9405	5.4153	24.654	33.882	68.903
		Scaled model	3.9405	5.4153	24.654	33.882	68.903
		Difference (%)	0.0003	0.0003	0.0003	0.0003	0.0003
	Direct	Scaled model	3.9400	5.4127	24.651	33.865	68.894
		Difference (%)	0.0129	0.0479	0.0129	0.0479	0.0129
Set 3	COMAC	Target	2.3044	3.1669	14.418	19.814	40.295
		Scaled model	2.3047	3.1670	14.420	19.815	40.300
		Difference (%)	0.0124	0.0036	0.0124	0.0036	0.0124
	Direct	Scaled model	2.3039	3.1725	14.414	19.849	40.285
		Difference (%)	0.0242	0.1769	0.0242	0.1769	0.0242
Set 5	COMAC	Target	23.044	31.669	144.18	198.141	402.949
		Scaled model	23.044	31.669	144.180	198.143	402.95
		Difference (%)	0.0003	0.0008	0.0003	0.0008	0.0003
	Direct	Scaled model	23.044	31.666	144.180	198.121	402.95
		Difference (%)	0.0001	0.0105	0.0001	0.0105	0.0001

Comparing the results obtained for the difference in the frequency values for each set, we can confirm

that COMAC does in fact result in better modal matching than when using direct modal matching. However the difference is not significant, and therefore both approaches can be used.

4.5.2 Reynolds Matching Analysis

With the objective of evaluating whether Reynolds number similarity is met, XFOIL is used. Reynolds and Mach numbers are calculated for the full-size wing and for the scaled model of each set. Then, XFOIL is used to evaluate if there are major differences in the curve L/D. Reynolds number values are calculated using Equation 2.3 and Mach number is calculated using Equation (2.2), for which the temperature value was chosen based on the altitude of the flight condition and according to ISA standard, the ratio of specific heat value was assumed 1.4 for air, and the specific gas constant assumed to be 287.058 J/kgK (value for dry air).

For Set 3, since the air conditions are not encountered naturally at any height, the temperature was calculated based on the ideal gas rule:

$$T = \frac{p}{R\rho}, \tag{4.50}$$

where p is the pressure of the air, considered to be 1 atm, R is the specific gas constant, and ρ is the density of the air obtained for this reduced model. The final temperature value is 73.71 K. The condensation temperature of air is 90.20 K, which means that it is not possible to have this conditions inside the wind-tunnel, and so the air properties of the reduced model will not correspond to the values obtained in the scaling procedure. Therefore, we will consider the temperature of 123.15 K as an approximation, for which the density and kinematic viscosity are 2.793 kg/m^2 and 3.08×10^{-6} m^2/s, respectively.

Since the flight condition is not the same for all sets of primary quantities, the full-size wing Reynolds and Mach numbers will also be different. The values for Reynolds and Mach number are listed in Table 4.14

Table 4.14: Reynolds and Mach numbers for the full-size wing flight condition considered for all Sets, and for the correspondent full-size wing.

		Reynolds Number	Mach Number
Sets 1, 3 and 5	Full-size Wing	2738960.3	0.1175
	Scaled Model Set 1	86637.7	0.0372
	Scaled Model Set 3	129870.1	0.0180
	Scaled Model Set 5	273972.6	0.1175
Set 2	Full-size Wing	547945.2	0.1356
	Scaled Model Set 2	547941.6	0.0687

The curves L/D for all sets and correspondent full-size wing are represented in Figure 4.3.

Analysing the curves, it is possible to see that with Set 2, for which the scaling factors were defined based on the attempt of matching the Reynolds number, the curve of the reduced model matches the one of the full-size wing as expected. For the other sets that does not happen. With a smaller Reynolds number, the viscosity in the air increases, leading to higher values of drag, which happens for Sets 1, 3 and 5.

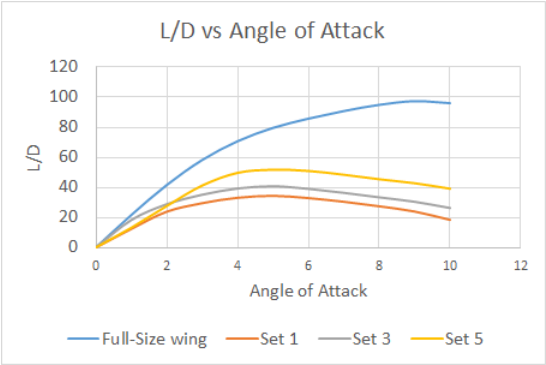

(a) L/D curves for Sets 1, 3, and 5, and the correspondent full-size wing

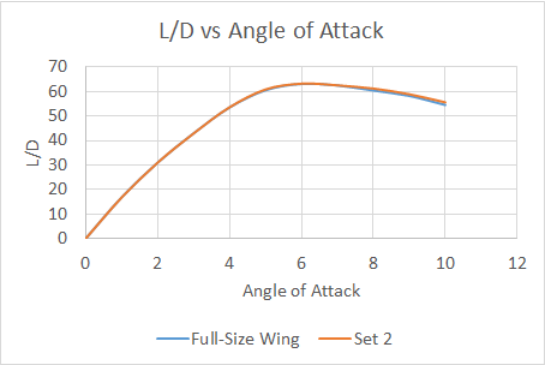

(b) L/D curves for Sets 2 and 4, and the correspondent full-size wing

Figure 4.3: L/D curves for all sets and the correspondent full-size wing.

Once the primary objective of aeroelastic scaling is to properly scale the aeroelastic response of the wing, drag forces are less important when compared to lift forces, which will have a higher contribution to the structural response of the wing.

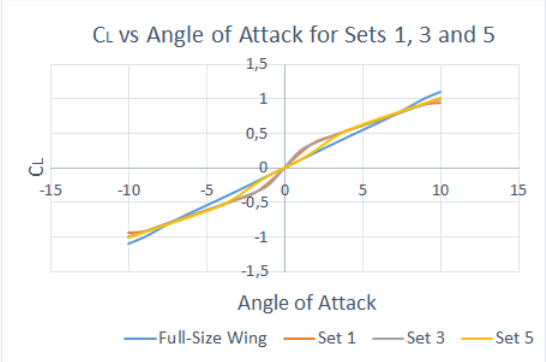

(a) C_L/α curve for Sets 1, 3, and 5, and the correspondent full-size wing

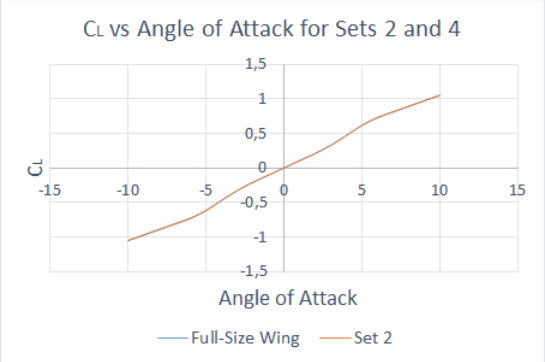

(b) C_L/α curve for Sets 2 and 4, and the correspondent full-size wing

Figure 4.4: C_L/α curve for all sets and the correspondent full-size wing.

Analysing Figure 4.4, in which C_L is represented in terms of angle of attack, one can see that there are some differences in C_L values between Sets 1, 3, and 5, and the correspondent full-size wing. For Sets 1 and 3, the relative error for C_L is higher than for Set 5, reaching 123.13% for an angle of attack of 1° for Set 3. For Set 5, the error in C_L is low when compared with Sets 1 and 3, reaching a maximum of 25.23% for an angle of attack of 3° . As for the C_D relative error for Set 5, the values range between 755.79% and 913.37%. Set 2 has very low relative errors both for the lift and drag coefficient.

In order to analyse whether the aerodynamic similarity would be met if the air properties in the air of the reduced model were respected for Set 3 (which would not be physically possible, as mentioned before), Reynolds and Mach number were calculated and L/D for different angles of attack obtained. It is possible to see that if it was possible to replicate the air properties, the aerodynamic similarity would be met for Set 3.

The major difference in the aerodynamic response happens for Set 1. This difference is also related to the size of the resulting reduced model.

Figure 4.5 shows the L/D curve for Set 3 considering the air properties obtained in the scaling procedure and for Set 1 with different length ratios.

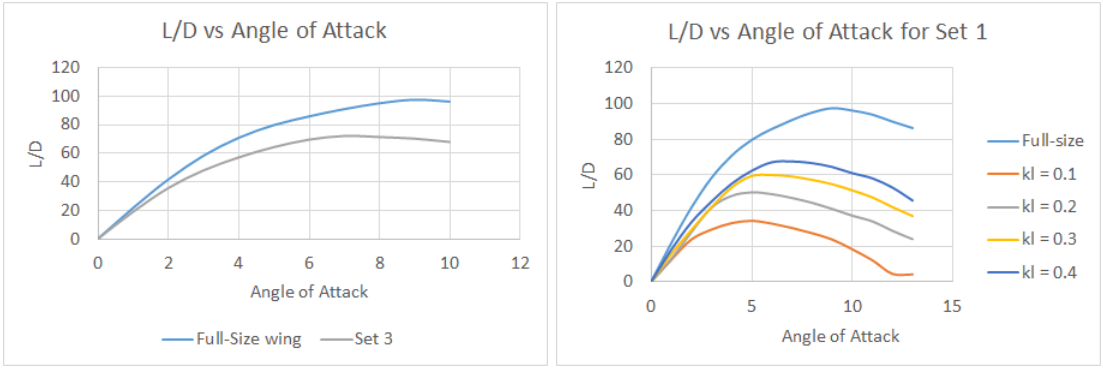

Figure 4.5: L/D curve for Set 3 considering the air properties obtained in the scaling procedure, and the correspondent full-size wing (left), and for Set 1 with different length ratios ($k_l = 0.1, 0.2, 0.3, 0.4$), and the correspondent full-size wing (right).

4.5.3 Primary Quantities Final Analysis

Analysing all the results obtained with the different sets of primary quantities one can conclude that there is no ideal choice, since all sets have their pros and cons.

Set 1 is the most useful set since it allows the choice of the velocity, span and density (even though in this analysis the velocity was not freely chosen, it is possible to do so). The negative side is that Reynolds and Mach number similarity are not met, which changes the aerodynamic performance and can affect the aeroelastic response. Despite that, the main difference is in the drag forces, and not lift forces, which could possible mean that the effects in the aeroelastic response are not that drastic.

For Set 2 the kinematic viscosity and density are primary quantities; that means that by properly defining the scaling factors, Reynolds similarity was possible to be achieved. The downside is that to accomplish a small span for the reduced model in order to fit the wind-tunnel installations not all cases are possible, reducing the utility of this set.

For Set 3 it is possible to choose the frequencies of the reduced model. This choice can be important since the measuring devices can only detect frequencies in a certain range. The problem is that the air properties of the reduced model resulted in properties that are not encountered in nature.

Using Set 4 of primary quantities, the optimization process was unable to obtain a feasible solution which respected the constraints imposed.

With Set 5 it is possible to choose the material, which does not happen with any of the other sets. It provides a good objective function value and reduced function calls. Mach number similarity was met, and despite the fact that the Reynolds number similarity is not met, the aerodynamic response of the reduced model was the closest one to the full-size wing, with relatively low errors in the C_L.

4.5.4 Methodologies Analysis

In order to compare which methodology is better, Methodology 2 was used considering Set 1 of primary quantities. Although proven well developed by recurring to Set 5, for which the final solution is known, Methodology 2 was not able to properly scale the full-size wing using Set 1. This is due to the fact that the material of the model is not well scaled (in Set 5, this does not happen since the scaling factors are calculated based on the matching of material properties), meaning that the deformation matching does not necessarily result in proper modal matching. In fact, optimization process 1 was able to provide a solution for the dimensions of the model section, but this solution was very different from the results obtained with Methodology 1. Using that solution, optimization process 2 was unable to provide a feasible result, since adding different masses to a beam do not alter the modal response to the extend needed. With this being said, it is possible to conclude that sequential scaling does not provide good results for overly simplified models.

Chapter 5

Laminated Composite Material Scaled Model

Composite materials are widely used in the aerospace industry, as mentioned before in Section 2.3. To verify if it is possible to obtain a reduced model made of laminated composite material that can replicate the scaled aeroelastic response of the full-size model, a scaling procedure was developed.

5.1 Full-Size Wing

The full-size wing used for this scaling analysis is the same used in the primary quantities analysis, which is described in Section 4.1.

5.2 Scaled Model

For the reduced model, a solidbeam with a rectangular cross-section is used, with 5 plies. In order to obtain a better value, hybrid composites are considered. These composites contain the same matrix material in all plies, but can have different fibre materials in each ply. The matrix material considered is Epoxy, for which material properties are listed in Table 5.1. For the fibre materials, 4 options are provided and listed in the same Table.

Table 5.1: Fibre and Epoxy material properties.

	Young's Modulus E (GPa)	Density ρ (kg/m^3)	Poisson Coefficient υ
Epoxy	4.5	1200	0.4
E-Glass Fibre	72	2550	0.21
S-Glass Fibre	86	2485	0.21
Kevlar 49	112	1450	0.36
Carbon IM7	300	1790	0.35

Since the composite beam is assumed symmetric, only the top 2 and middle plies's characteristics need to be defined as DV's.

5.3 Methodology

For this analysis, Set 1 of primary quantities is used. Since the full-size wing and the primary quantities values are the same, the scaling factors will also be the same and are listed in Table 4.6.

Methodology 1 is used. For the objective function, both approaches for matching the modal response are applied and compared. The constraints are the ones described by Equation (3.9), in which natural frequencies are used.

In a first optimization process, the DV's are: the thicknesses of the plies (t_i); the fraction of fibre in each ply (V_{f_i}); the orientation of the fibres in each ply (O_{r_i}); the width of the cross section (w); the fibre Young's Modulus of each ply (E_{f_i}); the fibre density of each ply (ρ_{f_i}); and the Poisson Coefficient of each ply (υ_{f_i}). Since the laminate is symmetric, DV's only need to be defined for plies 2, 1, and 0.

In order to guarantee that the fibre material properties correspond to a real material, the results are compared with the 4 options listed in Table 5.1. The material that provides the closest material properties values is selected.

Finally, a second optimization process is performed with the fibre materials defined, and not as DV's in order to optimize the geometric characteristics of the laminate.

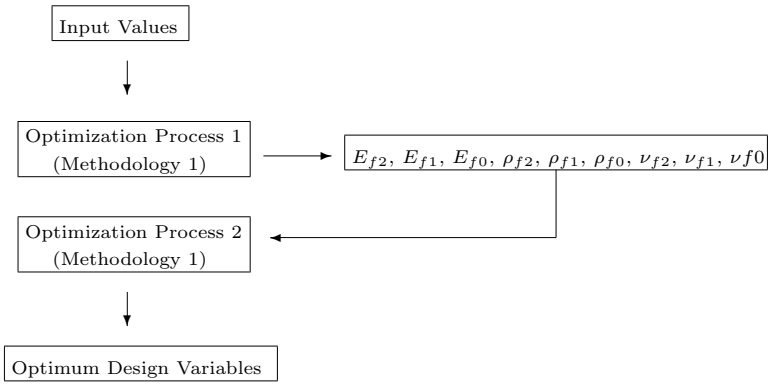

Figure 5.1: Scaling methodology algorithm for the analysis of a scaled model made of laminated composite materials.

Boundaries

Since there are some limitations in the characteristics of a laminated composite material, boundaries for the DV's correspondent to these characteristics must be defined.

For the volume fraction of fibre material, upper and lower boundaries are defined based on the critical and maximum practical volume fraction of fibre values. When the number of fibres present is too small, the stress on a composite may be high enough to break the fibres. The reinforcing action of the fibres is only observed once the fibre volume fraction exceeds the critical value ($V_f > V_{f,crit}$). As the fibre content increases, the strength of the composite increases proportionally. However, there is a practical maximum fibre content $V_{f,max,prac}$ above which composite properties deteriorate [45].

Aligned synthetic fibre reinforced composites, for example carbon/polyester, have a critical volume fraction of approximatelly 2.4% and a maximum practical volume fraction on the order of $75 - 80\%$. Despite that, since the fibres are meant to be aligned unidirectionally in each ply, and due to manufacturing

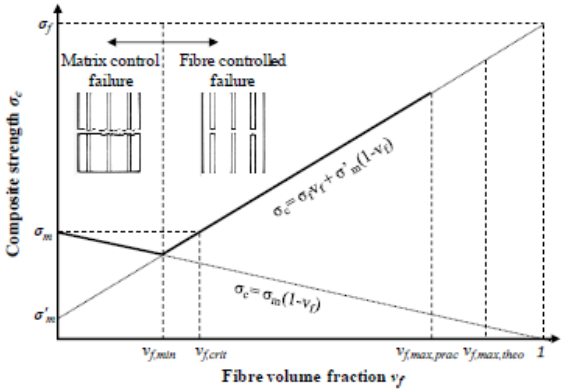

Figure 5.2: Schematic illustration of the variation of the strength of a unidirectional (brittle-fibre ductile-matrix) composite with fibre volume fraction [45]

aspects, the possible range of fibre volume fractions is $50 - 70\%$.

For the orientation of fibres in each ply, the limits are $-\pi/2$ and $\pi/2$. For the material properties of the fibres, the limits are based on the options provided.

All boundaries referent to the fibre characteristics are represented in Table 5.2.

Table 5.2: Fibre design variables boundaries.

DV's	Upper Boundary	Lower Boundary
Fibre volume fraction V_{f_i}	70	50
Fibre orientation O_{r_i} (rad)	$\pi/2$	$-\pi/2$
Fibre Young's Modulus E_{f_i} (GPa)	300	70
Fibre Density ρ_{f_i} (kg/m^3)	2600	1000
Fibre Poisson Coefficient υ_{f_i}	0.4	0.1

The boundaries for the thicknesses of each ply and the cross section length are defined by trial and error.

5.4 Results

The results obtained for the optimization of a reduced model made of hybrid composite materials using COMAC and direct modal matching are presented in Tables 5.3 and 5.4, respectively.

Despite the higher value of the final objective function in comparison with the previous results, the scaling procedure was able to properly scale the full-size wing to a reduced model made of hybrid composite materials using both approaches for matching the mode shapes. The COMAC graphic is represented in Figure 5.3, which is consistent with properly matched mode shapes.

However a proper result for the COMAC does not necessarily means proper frequency matching. And also, the minimum objective function value for each approach (COMAC and direct modal matching) can not be directly compared, as mentioned before. Therefore, a modal analysis is performed to the reduced model using the DV's obtained for both approaches. The results are presented in Table 5.5.

Analysing the frequencies that resulted from the reduced model optimum DV's using each approach, one can conclude that for this case, direct modal matching results in better modal matching. However

Table 5.3: Results obtained for the reduced model made of hybrid composite materials using COMAC.

	Optimization 1			**Optimization 2**	
	Initial DV's	Optimum DV's	Material Properties	Initial DV's	Optimum DV's
$t_2\ (m)$	0.0052	0.0045	-	0.0045	0.0020
$t_1\ (m)$	0.0026	0.0021	-	0.0021	0.0040
$t_0\ (m)$	0.0024	0.0027	-	0.0027	0.0030
V_{f_2}	0.5588	0.5889	-	0.5889	0.6877
V_{f_1}	0.5971	0.5960	-	0.5960	0.7000
V_{f_0}	0.5440	0.5657	-	0.5657	0.6648
$O_{r_2}\ (rad)$	1.1693	1.2717	-	1.2171	0.9670
$O_{r_1}\ (rad)$	1.0966	1.1672	-	1.1672	0.9024
$O_{r_0}\ (rad)$	0.3548	0.4883	-	0.4883	0.0376
$b\ (m)$	0.0248	0.0221	-	0.0221	0.0205
$E_{f_2}\ (GPa)$	300	292.16	300	-	-
$E_{f_1}\ (GPa)$	72	78.250	86	-	-
$E_{f_0}\ (GPa)$	112	109.78	112	-	-
$\rho_{f_2}\ (kg/m^3)$	1790	1478	1790	-	-
$\rho_{f_1}\ (kg/m^3)$	2550	2067	2485	-	-
$\rho_{f_0}\ (kg/m^3)$	1450	1792	1450	-	-
ν_{f_2}	0.3500	0.2179	0.3500	-	-
ν_{f_1}	0.2100	0.2242	0.2100	-	-
ν_{f_0}	0.3600	0.2701	0.3600	-	-
fval	0.1545		-	0.1521	
fcount	3983		-	3409	

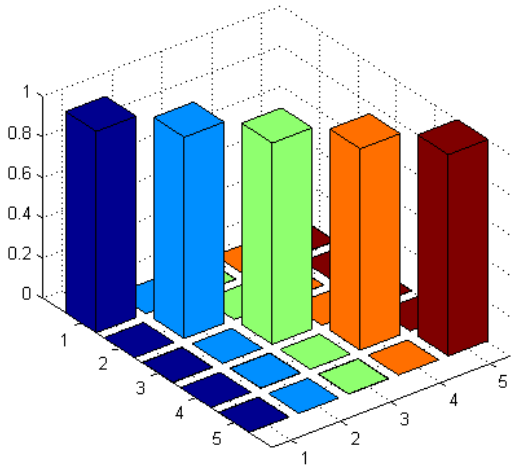

Figure 5.3: COMAC graphic for the laminate composite material reduced model optimization considering Set 1.

once again the difference is not significant, and so both approaches can be used. The number of finite element function calls needed to perform the optimization process using direct modal matching is lower than the COMAC approach (the COMAC approach needs 45.35.% more function calls), despite being higher when compared to a metallic reduced model due to the fact that there are more DV's involved.

Table 5.4: Results obtained for the reduced model made of hybrid composite materials using direct modal matching.

	Optimization 1			**Optimization 2**	
	Initial DV's	Optimum DV's	Material Properties	Initial DV's	Optimum DV's
t_2 (m)	0.0052	0.0052	-	0.0052	0.0052
t_1 (m)	0.0026	0.0026	-	0.0026	0.0026
t_0 (m)	0.0024	0.0024	-	0.0024	0.0024
V_{f_2}	0.5588	0.5589	-	0.5589	0.5593
V_{f_1}	0.5971	0.5971	-	0.5971	0.5972
V_{f_0}	0.5440	0.5439	-	0.5439	0.5444
O_{r_2} (rad)	1.1693	1.1699	-	1.1699	1.1715
O_{r_1} (rad)	1.0966	1.0930	-	1.0930	1.0878
O_{r_0} (rad)	0.3548	0.3507	-	0.3507	0.3541
b (m)	0.0248	0.0248	-	0.0248	0.0248
E_{f_2} (GPa)	300	299.91	300	-	-
E_{f_1} (GPa)	72	72.13	72	-	-
E_{f_0} (GPa)	112	112.23	112	-	-
ρ_{f_2} (kg/m^3)	1790	1788	1790	-	-
ρ_{f_1} (kg/m^3)	2550	2545	2550	-	-
ρ_{f_0} (kg/m^3)	1450	1451	1450	-	-
ν_{f_2}	0.3500	0.3496	0.3500	-	-
ν_{f_1}	0.2100	0.2097	0.2100	-	-
ν_{f_0}	0.3600	0.3592	0.3600	-	-
fval	0.1599		-	0.2399	
fcount	2231		-	1809	

Table 5.5: Frequencies comparison for Set 1 using a reduced model made of laminated composite material, and considering COMAC and direct modal matching.

			Natural Frequencies (Hz)					
			F1	F2	F3	F4	F5	Total Difference (%)
	Full-size wing		2.3044	3.1669	14.418	19.814	40.295	
	Mode shapes		1^{st} Flap	1^{st} Chord	2^{nd} Flap	2^{nd} Chord	3^{rd} Flap	
Set 1	COMAC	Target	7.2873	10.015	45.594	62.658	127.42	
		Scaled model	7.3128	9.9941	45.828	62.632	128.32	
		Difference (%)	0.3500	0.2050	0.5149	0.0410	0.7048	1.8157
	Direct	Scaled model	7.2652	10.010	45.530	62.730	127.49	
		Difference (%)	0.3030	0.0484	0.1392	0.1159	0.0494	0.6559

Chapter 6

Complex Wing

6.1 Full-Size Wing

A scaling procedure is applied to a more complex wing based on the NOVEMOR project of the EU FP7 reference wing, which was stretched to have a higher aspect-ratio of 16. The main geometric characteristics of the reference wing is listed in Table 6.1.

Table 6.1: Main geometric characteristics of the reference NOVEMOR wing.

Span b_{ref}(m)	31.46
First-half span $b_{1_{ref}}$ (m)	6.18
Second-half span $b_{2_{ref}}$ (m)	9.55
Wing area S_{ref} (m^2)	110
Mean Aerodynamic Chord MAC_{ref} (m)	4
Root Chord $c_{r_{ref}}$ (m)	7.57
Break Chord $c_{b_{ref}}$ (m)	3.99
Tip Chord $c_{t_{ref}}$ (m)	1.72
Sweep Angle $\Lambda_{LE_{ref}}$ ($^\circ$)	25
Dihedral Angle Γ_{ref} ($^\circ$)	4.5
Take-off Weight $W_{TO_{ref}}$ (kg)	58000

The new wing is designed to have an AR of 16, keeping the wing area, sweep angle, dihedral angle, take-off weight and engine weight values the same. Subscript ref and new stands for the reference and new wing geometric characteristics, respectively.

$$AR = 16 = \frac{b^2}{S} \Leftrightarrow b_{new} = \sqrt{ARS_{ref}} = 41.95, \tag{6.1}$$

$$MAC = \frac{S}{b} \Leftrightarrow MAC_{new} = \frac{S_{ref}}{b_{new}} = 2.62, \tag{6.2}$$

$$MAC_{new} = FMAC_{ref} \Leftrightarrow F = 0.654, \tag{6.3}$$

where F is a size factor.

With F it is possible to obtain the new root, break and tip chord values:

$$c_{r_{new}} = Fc_{r_{ref}} = 4.95, \tag{6.4a}$$

$$c_{b_{new}} = Fc_{b_{ref}} = 2.61, \tag{6.4b}$$

$$c_{t_{new}} = Fc_{t_{ref}} = 1.13. \tag{6.4c}$$

Finally, the first and second-half span values are obtained:

$$b_{1_{new}} = \frac{b_{1_{ref}}}{b_{ref}/2}\frac{b_{new}}{2} = 8.24, \tag{6.5a}$$

$$b_{2_{new}} = \frac{b_{new}}{2} - b_{1_{new}} = 12.73. \tag{6.5b}$$

The geometry of the new wing is illustrated in Figure 6.1 and its main characteristics are listed in Table 6.2.

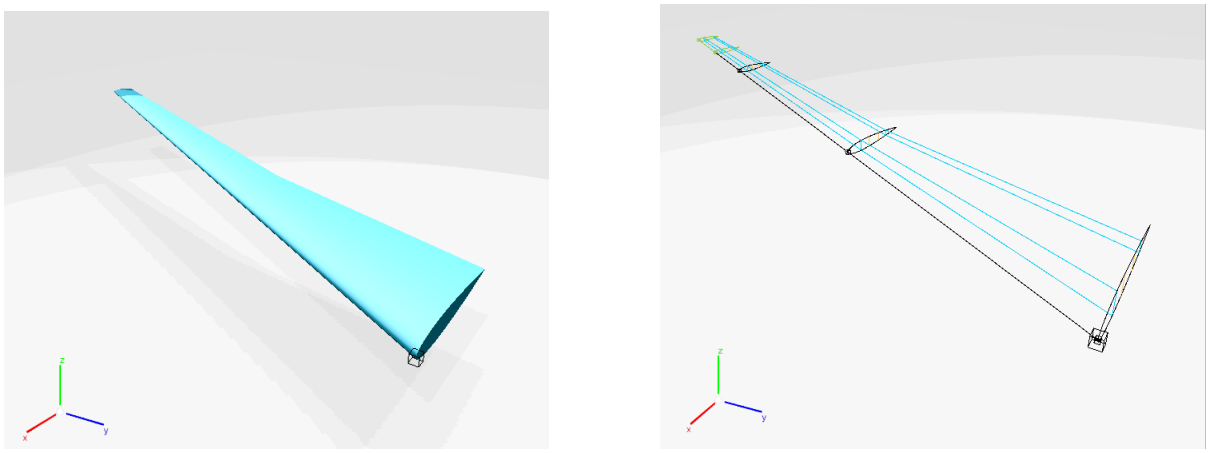

(a) Geometric shape

(b) Structural layout

Figure 6.1: Complex wing model geometric shape and structural layout.

Table 6.2: Geometric characteristics of the new wing.

Span b_{new}(m)	41.95
First-half span $b_{1_{new}}$ (m)	8.24
Second-half span $b_{2_{new}}$ (m)	12.73
Mean Aerodynamic Chord $M.A.C._{new}$ (m)	2.62
Root Chord $c_{r_{new}}$ (m)	4.95
Break Chord $c_{b_{new}}$ (m)	2.61
Tip Chord $c_{t_{new}}$ (m)	1.13

The wingbox model depicted in Figure 6.1 consists of a "square shape" box, in which the upper and lower layers follow the airfoil shape, instead of being straight. As for the side layers, they consist on the spars of the wing, which are placed at 25% and 75% of the local chord of the airfoil. The material of the wing is aluminium for which properties are presented in Table 4.1. The skin thickness t_s in the upper and lower layers is adimensionalized by the maximum thickness of the airfoil. As for the spars thickness

t_w, they are defined by the chord length. Constant spars and skins of 28.0 and 5.6 mm, respectively, were assumed for this model.

The dynamic analysis and scaling procedure are performed considering three flight conditions: cruise, alternate and hold. The angle of attack at which the analyses were computed was defined such that wing lift equals the weight of the aircraft (58 tons). The characteristics of each condition of flight are presented in Table 6.3. All the analyses conducted for this wing model were done using an in-house nonlinear aeroelastic framework [35]. This computational framework includes: a 3D panel model with compressibility and viscous corrections to model the aerodynamics; a 3D nonlinear condensed beam model for structural modelation; and a loosely-coupled Fluid-Structure Interaction algorithm responsible for computing the aeroelastic response in the time domain, as described in Section 3.3.

Table 6.3: Characteristics of the flight conditions for the full-size wing.

	Cruise	Alternate	Hold
Mach M	0.78	0.5	0.3
Altitude h (m)	11582.4	5486.4	609.6
Air density ρ (kg/m^3)	0.3320	0.6981	1.1549
Velocity V (m/s)	230.1546	159.2705	101.3838
Trim lift coefficient $C_{L_{trim}}$	0.5883	0.5841	0.8715
Trim angle of attack α_{trim} ($^\circ$)	5.3645	5.3267	7.9469

Both full-scale and reduced-scale models were defined considering the same aerodynamic and structural meshes. For the aerodynamic mesh the following distribution was set: 28 spanwise divisions; 40 chordwise divisions; and wake elements with lengths of 100 chords. Regarding the structural mesh, 50 nonlinear beam finite elements equally spaced in the span direction were considered.

6.2 Scaled Model

For the NOVEMOR wing, only Sets 1 and 5 were considered for the primary quantities selection. A 1/10th geometric scale was considered for devising the scaled model, which was defined with the same wingbox shape as the full-size wing (see Figure 6.1).

When considering Set 5, no optimization process was required since the wingbox thicknesses after applying the geometric scaling factor still are manufacturable (thicknesses of 2.80 mm and 0.56 mm, respectively, for the spars and skin of the reduced size model) using an aluminium material with the same properties of the full-scale, which was selected after setting density and pressure ratio equal to the unit.

For Set 1, the material selected is nylon, for which properties are listed in Table 6.4.

Table 6.4: Geometric characteristics of the new wing.

Young's Modulus (GPa)	1.27
Shear Modulus (GPa)	0.3
Density (kg/m^3)	1010
Yield stress (MPa)	35

6.3 Results

After selecting Set 5 and defining for the reduced-size model a $1/10^{th}$ length scale and the same material (*i.e.*, unitary density and pressure ratios), other important scaling factors can be derived to set the target values to be matched by the scaled model. Factors of 10 and 1 were respectively obtained for frequency and velocity, which means that the natural frequencies of the reduced-size model must be 10 times higher and the velocity has to be maintained to produce the same Mach number for the same air density. In terms of feasibility, the scaling down of the internal structure is achievable for this full-size internal structure; although difficulties may raise to reach the same Mach number, one has to decrease the air density and temperature which might only be attained in some wind tunnels.

Prior to compare the aeroelastic behaviour of both models, the aerodynamic and structural performance was evaluated. Table 6.5 shows the differences in C_L, C_D, C_M and natural frequencies between the two models. From this table, one can clearly see that the natural frequencies are exactly matched. Regarding the aerodynamic coefficients small differences were found, which are due to the fact that Reynolds number was not matched (accounted for in the implemented aerodynamic model through a viscous drag correction factor). The same mode shapes were found after visual identification, although the COMAC matrix is not exactly an identity matrix: some terms in the main diagonal are not unitary.

Table 6.5: Comparison of the aerodynamic and dynamic results between full and reduced models for Set 5.

	Aerodynamics									
	Cruise			Alternate			Hold			
	C_L (-)	C_D (-)	C_M (-)	C_L (-)	C_D (-)	C_M (-)	C_L (-)	C_D (-)	C_M (-)	
Full Scale	0.7792	0.0674	1.3048	0.6972	0.0141	1.0821	0.8711	0.0206	1.3813	
Target	0.7792	0.0674	1.3048	0.6972	0.0141	1.0821	0.8711	0.0206	1.3813	
Reduced Scale	0.7794	0.0660	1.3054	0.6989	0.0132	1.0846	0.8716	0.0195	1.3822	
Difference (%)	0.03	2.12	0.04	0.23	6.06	0.23	0.06	5.34	0.06	
	Natural Frequencies									
	F1 (Hz)	F2 (Hz)	F3 (Hz)	F4 (Hz)	F5 (Hz)	F6 (Hz)	F7 (Hz)	F8 (Hz)	F9 (Hz)	F10 (Hz)
Full Scale	1.2642	5.1286	5.2175	11.634	20.791	21.173	27.663	34.124	47.378	50.094
Target	12.642	51.286	52.175	116.34	207.91	211.73	276.63	341.24	473.78	500.94
Reduced Scale	12.642	51.286	52.175	116.34	207.91	211.73	276.63	341.24	473.78	500.94
Difference (%)	0.00	0.00	0.00	0.00	0.00	0.00	0.00	0.00	0.00	0.00
Mode Shapes	1^{st} Flap	2^{nd} Flap	1^{st} Chord	3^{rd} Flap	2^{nd} Chord	4^{th} Flap	1^{st} Torsion	5^{th} Flap	3^{rd} Chord	6^{th} Flap

The nonlinear aeroelastic response in the time domain was computed assuming the wing undeformed at the initial instance and released into a constant airflow, corresponding to each considered flight condition. A very good agreement was found between full and reduced scale models as one can notice in Figure 6.2, where the aeroelastic response measured at the wing tip in plunge, pitch and chord degrees-of-freedom is shown. In Figure 6.2, the reduced scale model results were converted to be comparable with those of the full-size model, after applying the length scaling factor for the deformations and time scaling factor for the time. The scaled model represents well the aeroelastic behaviour of the full-size model for the 3 different flight conditions, suggesting that with this aeroelastic scaling process it will be possible to explore the entire flight envelope using a reduced-size wind tunnel model. The discrepancies found are associated with the abovementioned viscous effects considering in the computational framework employed for the analyses.

Froude number similarity was not achieved in this scaling process: if it is used to define the airspeed for

each flight condition, different air loadings are obtained, thus rendering in different aeroelastic responses.

Table 6.6: Comparison of the aerodynamic and dynamic results between full and reduced models for Set 1.

	Aerodynamics									
	Cruise			Alternate			Hold			
	C_L (-)	C_D (-)	C_M (-)	C_L (-)	C_D (-)	C_M (-)	C_L (-)	C_D (-)	C_M (-)	
Full Scale	0.7792	0.0674	1.3048	0.6972	0.0141	1.0821	0.8711	0.0206	1.3813	
Target	0.7792	0.0674	1.3048	0.6972	0.0141	1.0821	0.8711	0.0206	1.3813	
Reduced Scale	0.7799	0.0678	1.3061	0.6977	0.0118	1.0893	0.8717	0.0190	1.3820	
Difference (%)	0.09	0.51	0.10	0.07	16.61	0.67	0.07	8.18	0.05	
	Natural Frequencies									
	F1 (Hz)	F2 (Hz)	F3 (Hz)	F4 (Hz)	F5 (Hz)	F6 (Hz)	F7 (Hz)	F8 (Hz)	F9 (Hz)	F10 (Hz)
Full Scale	1.2642	5.1286	5.2175	11.634	20.791	21.173	27.663	34.124	47.378	50.094
Target	2.7445	11.198	11.357	25.368	45.414	46.080	60.090	74.412	103.31	109.01
Reduced Scale	2.7118	10.584	11.662	23.490	41.826	43.160	52.560	67.103	93.734	96.325
Difference (%)	1.19	5.49	2.69	7.40	7.90	6.34	12.53	9.82	9.27	11.64
Mode Shapes	1^{st} Flap	2^{nd} Flap	1^{st} Chord	3^{rd} Flap	2^{nd} Chord	4^{th} Flap	1^{st} Torsion	5^{th} Flap	3^{rd} Chord	6^{th} Flap

For Set 1, the frequencies are not exactly matched with the ones of the full-size wing, and the discrepancies in the aerodynamic coefficients are higher than when considering Set 5 of primary quantities. Considering the air properties resulting from the scaling procedure, the discrepancies, both in the aerodynamic coefficients and frequencies, are higher.

Table 6.7: Comparison of the aerodynamic and dynamic results between full and reduced models for Set 1 considering the air properties provided by the scaling factors for hold and alternate.

		Aerodynamics								
		Alternate			Hold					
		C_L (-)	C_D (-)	C_M (-)	C_L (-)	C_D (-)	C_M (-)			
	Full Scale	0.6972	0.0141	1.0821	0.8711	0.0206	1.3813			
	Target	0.6972	0.0141	1.0821	0.8711	0.0206	1.3813			
	Reduced Scale	0.6074	0.0107	0.9426	0.8333	0.0183	1.3210			
	Difference (%)	12.89	24.22	12.89	4.35	11.30	4.36			
		Natural Frequencies								
	F1 (Hz)	F2 (Hz)	F3 (Hz)	F4 (Hz)	F5 (Hz)	F6 (Hz)	F7 (Hz)	F8 (Hz)	F9 (Hz)	F10 (Hz)
Full Scale	1.2642	5.1286	5.2175	11.634	20.791	21.173	27.663	34.124	47.378	50.094
Target	2.7445	11.198	11.357	25.368	45.414	46.080	60.090	74.412	103.31	109.01
Reduced Scale	3.8465	11.321	11.635	23.100	24.030	36.705	41.495	45.931	65.918	70.851
Difference (%)	40.15	1.10	2.45	8.94	47.09	20.35	30.94	38.28	36.19	35.00
Mode Shapes	1^{st} Flap	2^{nd} Flap	1^{st} Chord	3^{rd} Flap	2^{nd} Chord	4^{th} Flap	1^{st} Torsion	5^{th} Flap	3^{rd} Chord	6^{th} Flap

Considering Set 1 the Mach number similarity was not achieved, resulting in a poor matching of the aerodynamic and structural response for the alternate and hold flight conditions. Therefore, the properties of the air (density and temperature) were altered in order to provide Mach number similarity for these cases. For cruise condition, the air properties did not need to be changed. The results are presented in Table 6.6 and Figure 6.3.

Results obtained considering the air properties resultant from the scaling factors for alternate and hold are presented in Table 6.7 and Figure 6.4.

By matching Froude number for Set 1, the velocity scaling factor did not have into account the Mach number similarity, resulting in poor matching of aerodynamic and structural responses. This could imply that, despite being considered as mandatory in aeroelastic scaling, Froude number similarity provides worse results than when Mach number similarity is considered. This also happens for the simplified model analysis when comparing the different sets of primary quantities and the parameters for which each set's velocity scaling factor is defined.

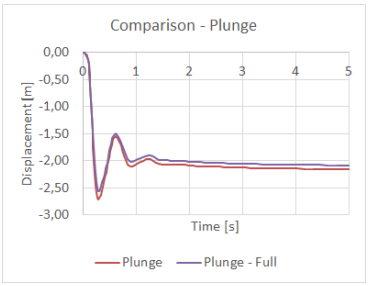

(a) Cruise Plunge

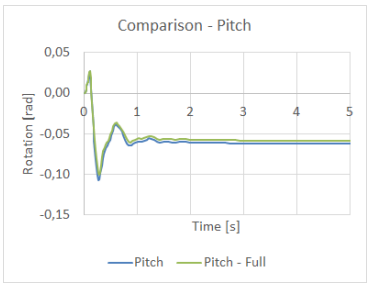

(b) Cruise Pitch

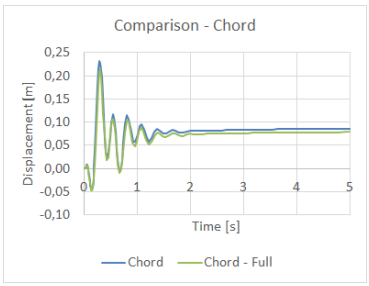

(c) Cruise Chord

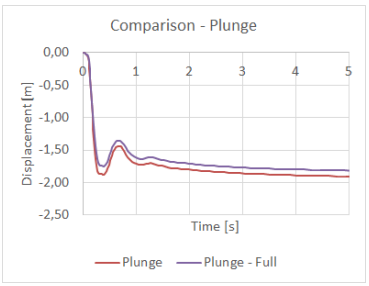

(d) Alternate Plunge

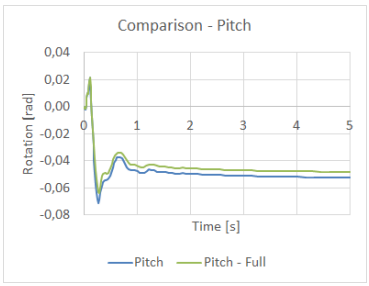

(e) Alternate Pitch

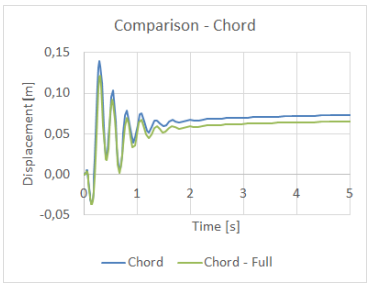

(f) Alternate Chord

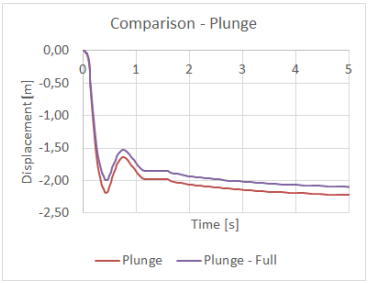

(g) Hold Plunge

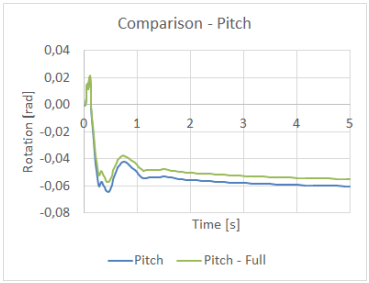

(h) Hold Pitch

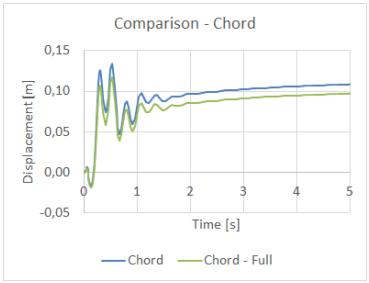

(i) Hold Chord

Figure 6.2: Comparison of the aeroelastic response measured at the wing tip for plunge, pitch and chord degrees-of-freedom for the reduced and full size aircraft for Set 5.

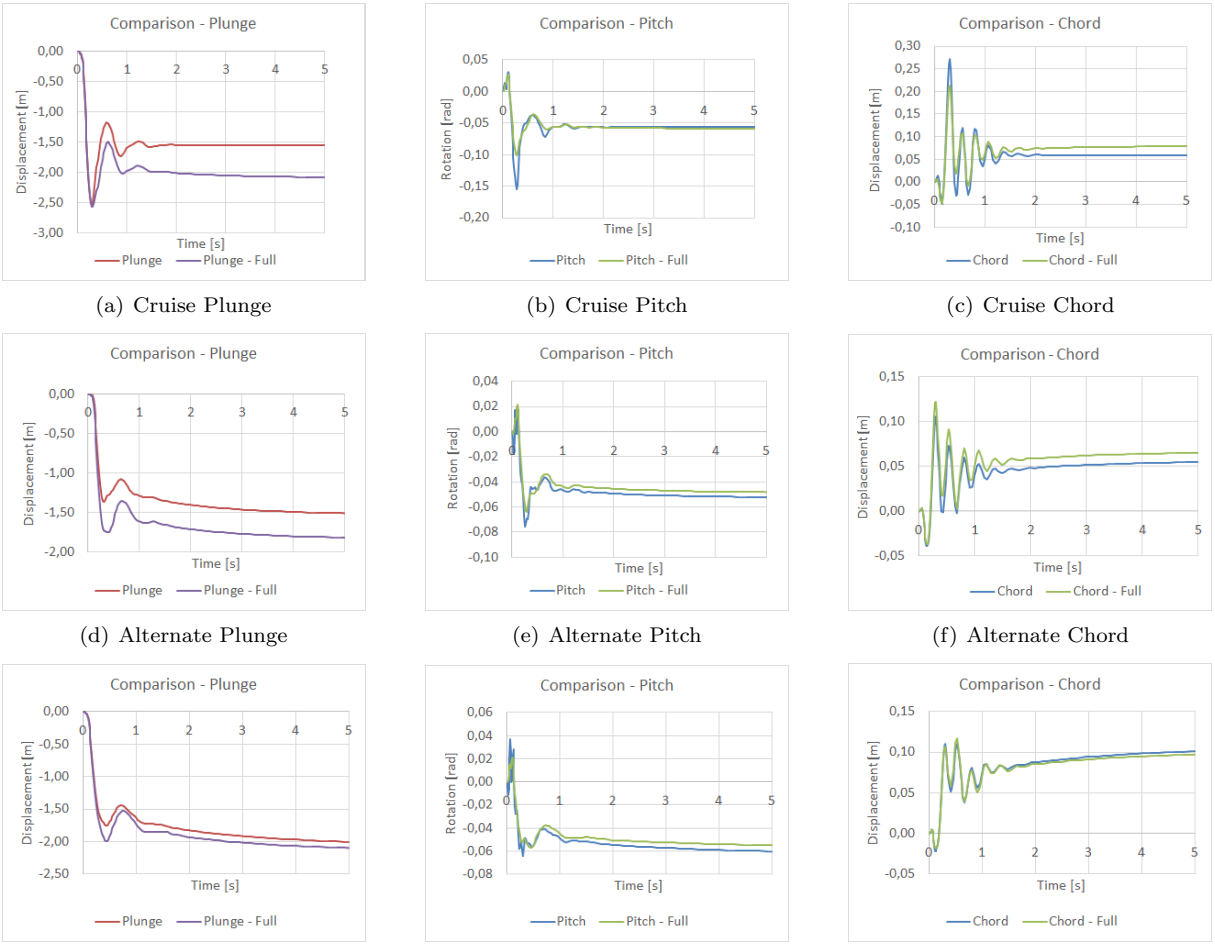

(a) Cruise Plunge (b) Cruise Pitch (c) Cruise Chord

(d) Alternate Plunge (e) Alternate Pitch (f) Alternate Chord

(g) Hold Plunge (h) Hold Pitch (i) Hold Chord

Figure 6.3: Comparison of the aeroelastic response measured at the wing tip for plunge, pitch and chord degrees-of-freedom for the reduced and full size aircraft for Set 1.

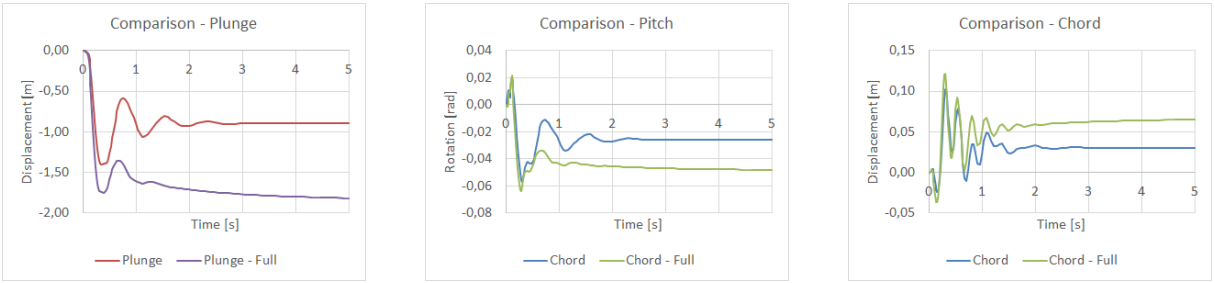

(a) Alternate Plunge (b) Alternate Pitch (c) Alternate Chord

(d) Hold Plunge (e) Hold Pitch (f) Hold Chord

Figure 6.4: Comparison of the aeroelastic response measured at the wing tip for plunge, pitch and chord degrees-of-freedom for the reduced and full size aircraft for Set 1 considering the air properties provided by the scaling factors.

Chapter 7

Conclusions

This work consisted in analysing the effects that different choices in the aeroelastic scaling procedures have on the results. An analysis on different sets of primary quantities, different materials and structures, and also different methodologies was done.

Concerning the primary quantities set, it was concluded that Sets 1 and 5 are the most useful since the other sets have some contraints. Comparing Sets 1 and 5, one can conclude that Mach number similarity could be more relevant to aeroelastic scaling than Froude number similarity, since Set 1, which respects the Froude number similarity, has the most differences in the aerodynamic response and frequencies analysis when compared to Set 5, for which Mach number similarity is met, and not Froude number. Also, the same trim condition has a beneficial impact on the results, since Set 3, which respects the trim condition and not the Froude number similarity, has a better objective function value and aerodynamic response (even when the air conditions of the reduced model are not respected) than Set 1 and 2.

Analysing the different methodologies developed, it was concluded that for simple models, for which the material is not scaled, a sequential matching of the stiffness and mass distribution does not provide good results.

Comparing the approaches used to match the modal response of the reduced model to the scaled modal response of the full-size wing, it was not possible to reach a conclusion on which approach is better, since the differences were not significant and also the number of test cases is not sufficient.

Considering laminated composite materials for the reduced model, it was possible to properly scale a simple full-size wing model, despite the relatively high value of the objective function. Also the computational time is much higher, which means that by adding complexity to the full-size wing and reduced model would be computationally difficult to complete the optimization processes, due to the high number of DV's.

Finally, when considering a more complex wing, Set 5 of primary quantities provided good results, despite the non-similarity of the Froude number. As it was concluded before, this could possibly mean that Froude number similarity may not be that relevant, and that Mach number similarity (which is met in this case) can provide good results.

7.1 Future Work

In future work, Sets 1 and 5 could be further explored in order to try and match the aerodynamic response of the reduced model to the full-size wing. Despite the issues with manufacturing, composite materials proved to be a material to have into account for aeroelastic scaled models and an analysis in more complex structures should be done respecting constraints imposed due to manufacturing. Also, an analysis and possible optimization of the structural response of the hybrid composite scaled model resultant from the scaling process should be performed.

Bibliography

[1] I. H. Abbott and A. E. Von Doenhoff. *Theory of wing sections, including a summary of airfoil data.* Dover Publications Inc., New York, 1959.

[2] C. Spada, F. Afonso, F. Lau, and A. Suleman. Aeroelastic analysis of high aspect-ratio wings. In *54th AIAA Aerospace Sciences Meeting, AIAA Science and Technology Forum and Exposition (SciTech 2016)*, San Diego, California, January 2016.

[3] Z. Wan and C. E. Cesnik. Geometrically nonlinear aeroelastic scaling for very flexible aircraft. *AIAA Journal*, 52(10):2251–2260, Jul 2014.

[4] G. A. P. Dewey H. Hodges. *Introduction to Structural Dynamics and Aeroelasticity.* Cambridge University Press, Cambridge, 2^{nd} edition, 2014.

[5] E. Buckingham. On physically similar systems; illustrations of the use of dimensional equations. *Phys. Rev.*, 4:345–376, Oct 1914. doi: 10.1103/PhysRev.4.345. URL `http://link.aps.org/doi/10.1103/PhysRev.4.345`.

[6] R. L. Bisplinghoff, H. Ashley, and R. L. Halfman. *Aeroelasticity.* Dover Publications, Inc., 31 East 2nd Street, Mineola, N.Y. 11501, 1996.

[7] M. Blair, D. Garmann, R. Canfield, V. Bond, P. Pereira, and A. Suleman. Non-linear aeroelastic scaling of a joined-wing concept. In *48th AIAA/ASME/ASCE/AHS/ASC Structures, Structural Dynamics, and Materials Conference*, volume 1887, Honolulu, Hawaii, April 2007.

[8] M. French. An application of structural optimization in wind tunnel model design. In *31st Structures, Structural Dynamics and Materials Conference*, pages 134–137, 1990.

[9] M. French and F. Eastep. Aeroelastic model design using parameter identification. *Journal of Aircraft*, 33(1):198–202, Jan-Feb 1996.

[10] P. Friedmann and E. Presente. Active control of flutter in compressible flow and its aeroelastic scaling. *Journal of Guidance, Control, and Dynamics*, 24(1):167–175, Jan-Feb 2001.

[11] P. Pereira, L. Almeida, A. Suleman, V. Bond, R. Canfield, and M. Blair. Aeroelastic scaling and optimization of a joined-wing aircraft concept. In *48th AIAA/ASME/ASCE/AHS/ASC Structures, Structural Dynamics, and Materials Conference*, page 1889, Honolulu, Hawaii, April 2007.

[12] V. L. Bond, R. A. Canfield, A. Suleman, and M. Blair. Aeroelastic scaling of a joined wing for nonlinear geometric stiffness. *AIAA Journal*, 50(3):513–522, Mar 2012.

[13] A. P. Ricciardi, R. A. Canfield, M. J. Patil, and N. Lindsley. Nonlinear aeroelastic scaling of a joined-wing aircraft. In *53rd AIAA/ASME/ASCE/AHS/ASC structures, structural dynamics and materials conference, AIAA*, volume 1454, Honolulu, Hawaii, April 2012.

[14] A. P. Ricciardi, C. A. Eger, R. A. Canfield, and M. J. Patil. Nonlinear aeroelastic-scaled-model optimization using equivalent static loads. *Journal of Aircraft*, 51(6):1842–1851, Nov-Dec 2014.

[15] B. Tang, Z. Wu, and C. Yang. Aeroelastic scaling laws for gust load alleviation control system. *Chinese Journal of Aeronautics*, 29(1):76–90, 2015.

[16] P. Shyprykevich. Characterization of graphite/epoxy laminates for aeroelastic tailoring. In *Composite Materials: Testing and Design (Fifth Conference) ASTM STP 674*, pages 40–56, 1979.

[17] C. E. Cesnik, D. H. Hodges, and M. J. Patil. Aeroelastic analysis of composite wings. In *Proceedings of the 37th Structures, Structural Dynamics, and Materials Conference*, Salt Lake City, UT, U.S.A, April 1996.

[18] Z. Wan, Y. Hong, D. Liu, and Y. Chao. Aeroelastic analysis and optimization of high-aspect-ratio composite forward-swept wings. *Chinese Journal of Aeronautics*, 18(4):317–325, Nov 2005.

[19] M. Kameyama and H. Fukunaga. Optimum design of composite plate wings for aeroelastic characteristics using lamination parameters. *Computers and Structures*, 85(3):213–224, 2007.

[20] O. Stodieck, J. E. Cooper, P. M. Weaver, and P. Kealy. Improved aeroelastic tailoring using tow-steered composites. *Composite Structures*, 106:703–715, 2013.

[21] A. Collar. The expanding domain of aeroelasticity. *Journal of the Royal Aeronautical Society*, 50 (428):613–636, 1946.

[22] C. Wyatt Emory. *Prediction of Limit Cycle Oscillation in an Aeroelastic System using Nonlinear Normal Modes*. PhD thesis, Faculty of the Virginia Polytechnic Institute and State University, 2010.

[23] R. W. Bunton and C. M. Denegri Jr. Limit cycle oscillation characteristics of fighteraircraft. *Journal of Aircraft*, 37(5):916–918, 2000.

[24] J. Richards. *An Experimental Investigation of a Joined Wing Aircraft Configuration Using Flexible, Reduced Scale Flight Test Vehicles*. PhD thesis, University of Victoria, 2014.

[25] C. E. Cesnik. Workshop on nonlinear aeroelasticity and flight dynamics of very flexible aircraft. November 2015.

[26] J. N. Reddy. *Mechanics of laminated composite plates and shells: theory and analysis*. CRC press, Boca Raton, Florida, 2004.

[27] M. Sreekala, J. George, M. Kumaran, and S. Thomas. The mechanical performance of hybrid phenol-formaldehyde-based composites reinforced with glass and oil palm fibres. *Composites science and technology*, 62(3):339–353, 2002.

[28] J. Zhang, K. Chaisombat, S. He, and C. Wang. Glass/carbon fibre hybrid composite laminates for structural applications in automotive vehicles. In *Proceedings of the* 4^{th} *International Conference of Sustainable Automotive Technologies*, Orlando Florida, 1996.

[29] R. Pruthviraj. A review on recent applications and future prospectus of hybrid composites in various engineering applications. *Chemical Technology*, 9(3), 2014.

[30] M. M. Thwe and K. Liao. Durability of bamboo-glass fiber reinforced polymer matrix hybrid composites. *Composites Science and Technology*, 63(3):375–387, 2003.

[31] J. Nocedal and S. Wright. *Numerical Optimization*. Springer Series in Operations Research, Springer Verlag, 2^{nd} edition, 2006.

[32] R. J. Allemang. The modal assurance criterion–twenty years of use and abuse. *Sound and vibration*, 37(8):14–23, 2003.

[33] Z. Ugray, L. Lasdon, J. Plummer, F. Glover, J. Kelly, and R. Martí. Scatter search and local nlp solvers: A multistart framework for global optimization. *INFORMS Journal on Computing*, 19(3): 328–340, 2007.

[34] How globalsearch and multistart work. `https://www.mathworks.com/help/gads/how-globalsearch-and-multistart-work.html`. [Online; accessed 15-May-2016].

[35] A. Suleman, F. Afonso, J. Vale, E. Oliveira, and F. Lau. Non-linear aeroelastic analysis in the time domain of high-aspect-ratio wings: Effect of chord and taper-ratio variation. *The Aeronautical Journal*, 2016.

[36] J. N. Reddy. *An introduction to the finite element method*, volume 2. McGraw-Hill New York, 1993.

[37] O. Zienkiewicz. *The Finite Element Method in Engineering Science*. 3^{rd} edition.

[38] K. Bathe. *Finite Element Procedures in Engineering Analysis*. Prentice-Hall, New Jersey, 1982.

[39] S. Lee. *MSC/NASTRAN Nonlinear Analysis*, volume I. The MacNeal-Schwendler Corporation, 1992.

[40] L. L. Erickson. Panel methods: An introduction. Technical report, NASA, 1990.

[41] J. Katz and A. Plotkin. *Low-speed aerodynamics*, volume 13. Cambridge University Press, 2001.

[42] Y. Bazilevs, K. Takizawa, and T. Tezduyar. *Computational Fluid-Structure Interaction: Methods and Applications, Wiley Series in Computational Mechanics.* John Wiley Sons, Ltd, New York, 1^{st} edition, 2013.

[43] J. E. Ballmann. *Flow Modulation and Fluid-Structure Interaction at Airplane Wings, Part of the series Numerical Fluid Mechanics and Multidisciplinary Design*, volume 84. Springer, Berlin, 1^{st} edition, 2003.

[44] D. Hodges and G. Pierce. *Introduction to Structural Dynamics and Aeroelasticity.* Press Syndicate of the University of Cambridge, Cambridge, UK, 1996.

[45] D. U. Shah, P. J. Schubel, P. Licence, and M. J. Clifford. Determining the minimum, critical and maximum fibre content for twisted yarn reinforced plant fibre composites. *Composites Science and Technology*, 72(15):1909–1917, 2012.